공학박사학위논문

건설기계 프레임의 통합 위상 최적화

Integrated topology optimization
for construction equipment frame

2015년 8월

서울대학교 대학원

기계항공공학부

곽 성 규

Abstract

Integrated Topology Optimization for Construction Equipment Frame

Sung Kyu Kwak
Department of Mechanical and Aerospace Engineering
The Graduate School
Seoul National University

The research in this dissertation aims to develop an integrated structural topology optimization method applicable to the design of a construction equipment frame. There are two major design issues existing in the industry; one is the simultaneous design of an actuator layout and structural topology of the frame and the other, to consider the manufacturing aspect of the topology optimization result. The embedded actuators in the construction equipment, such as steering cylinders in a wheel loader, transmit external forces to the frame. Because the location of an actuator acts as a loading point in the structure, the optimized structure can be significantly affected by the loading location. Moreover, when the actuator layout is not yet determined at the early concept stage of the frame design, the location of the actuator is allowed to move in a designated design domain. This motivates simultaneous optimization of a loading point and structural topology and this study presents a method to achieve this goal. There have been a few related efforts about the simultaneous optimization of a loading point and structural

topology, but the loading point is limited only along a given line or boundary. Even if an optimized layout is found through topology optimization, the actual manufacturing of an optimal structure by welding is a major obstacle because the welding path by the optimization is unrealistic. To overcome this difficulty, we propose a so-called plate-like topology optimization, which extracts the topological layouts of nodal design variables projected on the specified plane along the pre-determined direction. This approach makes the topologically optimized results amenable to the welded structure.

The simultaneous optimization method of a loading point and structural topology and the method to consider the weld manufacturability are implemented by using *Matlab* and *Abaqus*. After verification examples are considered, the optimal design of a wheel loader frame is dealt with in order to show the practicality of the proposed method in industrial engineering problems.

Keywords: Topology optimization, Simultaneous optimization, Movable load, Stiffness design, Weld manufacturing constraint

Student Number: 2011-31289

Contents

List of Figures

Chapter 1.

Introduction

Topology optimization [1-3] is a well-established and innovative design methodology successfully applied in various areas of industry. The concept of topology optimization is recognized as structural layout optimization to find such an optimized material distribution in the design domain to maximize the performance function (e.g. structural stiffness) with satisfying constraints such as specified volume and modal frequency. Although important achievements continue to motivate further studies about the applications of topology optimization and its capabilities in solving complex engineering design problems [4-23], but unfortunately there are little works reported in the design of construction equipment frame. Recently, the regulation of greenhouse gas emission and efforts for reduction of the total cost ownership require fundamental re-design of the frame structure. Weight reduction maintaining the structural performance becomes an important topic in this situation, and thus, topology optimization as an innovative design methodology gets much attention than ever before.

There are some issues in the application of the topology optimization to the construction equipment industry. Figure 1.1 shows a typical wheel loader, one of widely used construction equipment, and the frame of a wheel loader. Generally, construction equipment has actuators for the operation of desired work, and therefore, the load transmitted from them configures fundamental load cases of the frame. In this situation,

the location of actuators can change the structural topological layouts considerably. If there is a freedom in the early conceptual design stage to modify the actuator layout for the structural performance, we should consider the determination of the structural layout and the actuator layout at the same time. This first issue requires the simultaneous optimization method for the structural design and actuator layout. Another issue is about manufacturing aspect because the frame of construction equipment is mainly composed of relatively thin plates. It is usually fabricated by the seam-weld process which is difficult to effectively derive the detailed shape design from the result of the topology optimization, which is a truss structure typically. In this study, topology optimization method considering above mentioned issues is investigated for the application to the design of the construction equipment frame.

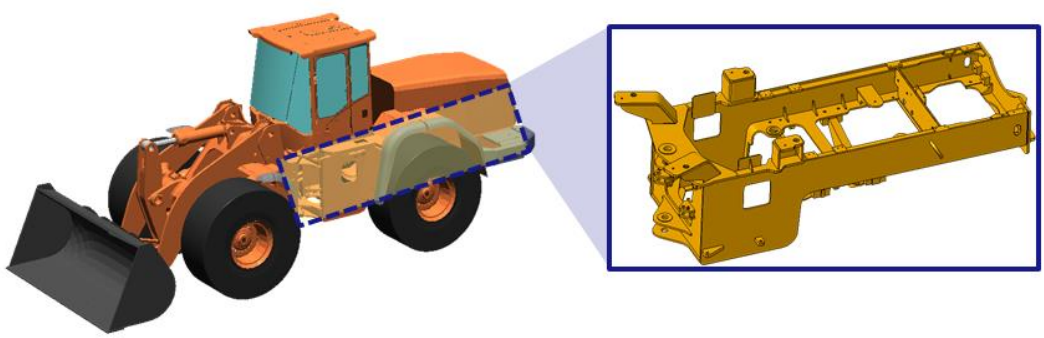

Fig. 1.1 Illustration of a wheel loader

In the standard structural topology optimization, it is common to find out the optimal material layout with all loading conditions, such as the magnitude, direction and location of an applied load, specified [2, 4, 6, 16, 18]. This kind of formulation has been widely

accepted in various applications. But, the simultaneous optimization of the actuator position and structural topology corresponds to the determination of the loading location in standard structural optimization problem because actuators transmit the load the frame structure. As the actuator layout changes, the specific loading location in the frame can be considered to move. Therefore, we propose to relax the topology optimization problem by allowing the applied load to move in the design domain.

There were some earlier works related to the present subject. Simultaneous design of boundary and structural topology [24] was developed by adding spring element to the possible points for the boundary in continuum domain. Support location design problem in the topology optimization framework [25] was considered to determine the discrete optimal support location to maximize structural compliance. For the simultaneous design of the loading condition and structure, Fuchs and Moses [26] first suggested a topology optimization by the SIMP (Solid Isotropic Material with Penalization) method to minimize the structural compliance with a load that is allowed to move along the loading direction. Alternative or extended methods were also investigated using ESO (Evolutionary Structural Optimization) method [27, 28]. In these works, the notion of a transmissible load was introduced to define a load of a given magnitude and direction which can move along its line of action [29, 30]. Most recently, Zhang *et al.* [31] considered movable cases by allowing the loading location to move along any specific loading line including a boundary line of the design domain. While the aforementioned researches were apparently concerned with the simultaneous optimization of a structural topology and loading location moving in the line, no work has been reported to deal with

the case where the loading location can freely move to any location within a design domain. The simultaneous optimization problem considered in this study, as schematically illustrated in Fig. 1.2, is to determine a loading location and structural topological layout for compliance minimization under a general movable load condition; while the magnitude and direction of an applied load is fixed, the location of an applied load is allowed to move anywhere, actually any node, inside the discretized design domain or along its domain boundary. To be able to solve this type of problems, a new method will be developed and tested in this study.

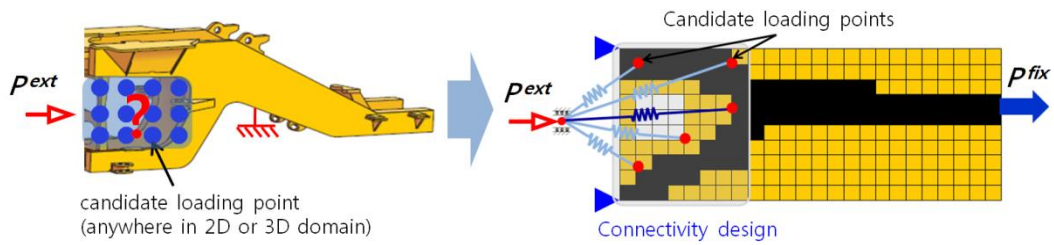

Fig. 1.2 Schematic illustration of the proposed simultaneous optimization

There have been several efforts [32-35] for the manufacturing constraint, such as casting, extrusion and draw direction, in the topology optimization. Among them, topology optimization method suggested by Leiva [33] has the similar characteristics applicable to the welded structure. While the method is originally for the casting constraint in the topology optimization, it can generate plate-like structure rather efficiently which is necessary for the welded structure. From this point, modifications and extensions of the plate-like topology optimization method are implemented in this study.

For the specific optimization problem motivated by the actual engineering practice, structural design of the construction equipment frame, large size of problem should be treated efficiently. Thus, the developed optimization method should be implemented with the commercial finite element analysis software, e.g. *Abaqus*. In this work, in-house topology optimization code using the *Matlab* - *Abaqus* interface is developed and tested for the design of a wheel loader frame. A simplified design example of a wheel loader frame hosting a steering actuator is actually solved here, which will clearly demonstrate the usefulness of the present investigation.

In chapter 2, standard topology optimization problem for a typical wheel loader frame is formulated and numerical studies are conducted using the commercial optimization software *OptiStruct*. The design issues in the application of the standard topology optimization are discussed. Feasibility study for the proposed simultaneous optimization is checked in the wheel loader frame model.

Chapter 3 is mainly dedicated to the proposition of new topology optimization method of simultaneous determination of an actuator position and structural topological layouts. Specific modeling technique for the correct load transfer in the movable loading location design problem is described. Moreover, formulation for the simultaneous optimization is proposed. The developed optimization method is verified and validated with several benchmark problems. A design example of simplified wheel loader frame in two-dimensional domain is demonstrated to show the possibility to the engineering practices. Examples in three-dimensional domain are then followed.

In chapter 4, topology optimization method considering weld manufacturability is developed with the use of the *Matlab – Abaqus* interface. Thereafter, integrated with the simultaneous optimization method developed in chapter 3, design examples of the simultaneous optimization of an loading location and structural topology considering weld manufacturability are demonstrated. One of the examples is a simplified structural design of actual wheel loader frame. The usefulness of the proposed optimization method will be revealed in this chapter.

Finally, conclusion of the thesis is made in chapter 5.

Chapter 2.

Standard topology optimization and design issues

2.1 Chapter overview

In this chapter, standard topology optimization of a wheel loader frame is studied and related issues in the application to the construction equipment frame will be discussed. A wheel loader frame, as shown in Fig. 2.1, is fabricated by conventional welding process; the results from standard topology optimization should be interpreted to the detailed welded structure by the design engineer. Possibilities of standard topology optimization to the practical design of frame structure should be checked in the view point of the manufacturability. In the next section, standard topology optimization problem for the wheel loader frame to enhance the performance of the structure will be examined and discussed.

Moreover, similar design issues of wheel loader frames can be found through comparison with several typical frames. They are actuator (steering cylinder) layout design and section shape of the side member in the frame structure. The actuator layout corresponds to the loading location in the design domain as mentioned in the previous chapter. The latter issue is related to the manufacturing aspect because the section shape of side member in frame structure should be so determined as to be fabricated with the welding process.

The issue of manufacturability is obvious, but impact of the actuator layout on the structural topology of the frame should be checked previously. Before detailed description on the simultaneous optimization of a actuator layout and structural topology, feasibility study on the layout design of the frame structure will be made in this chapter.

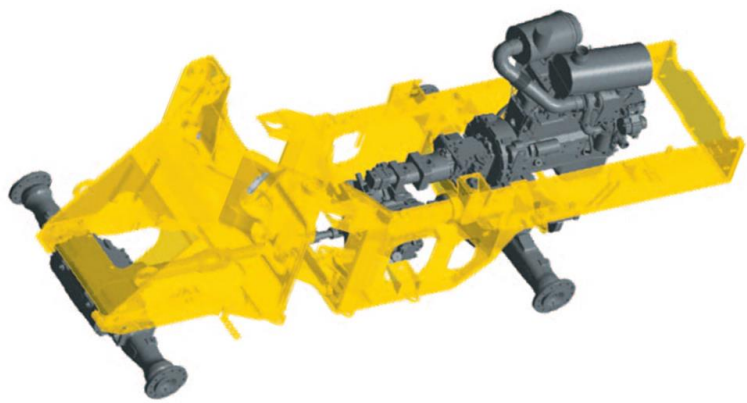

Fig. 2.1 Illustration of a typical wheel loader frame

2.2 Finite element model setup of a wheel loader frame

Figure 2.2 shows the finite element model of a typical wheel loader rear frame. For the purpose of topology optimization, design domain is filled with continuum elements in order to assign as much freedom as possible to the optimization algorithm. There are several main components mounted on the frame; cabin, hydraulic tank, fuel tank, axle, engine, transmission, and counter weight. They are connected via rigid elements in Fig. 2.2. Specific value of the mass and inertia of these components cannot be listed due to

the security reason of the manufacturing company. The typical load cases for the static analysis, which comes from the major deflection mode of the frame, is shown in Fig. 2.3. Numerical values of the load cases are not detailed also. Works loads are transmitted to the pin joints in the front part of the frame and steering cylinder forces, to the brackets in the both side of the front part. Fatigue strength is not considered in this study, because the object of this study is to maximize the structural stiffness. It is more general to consider the fatigue resistance in size/shape optimization stage [5].

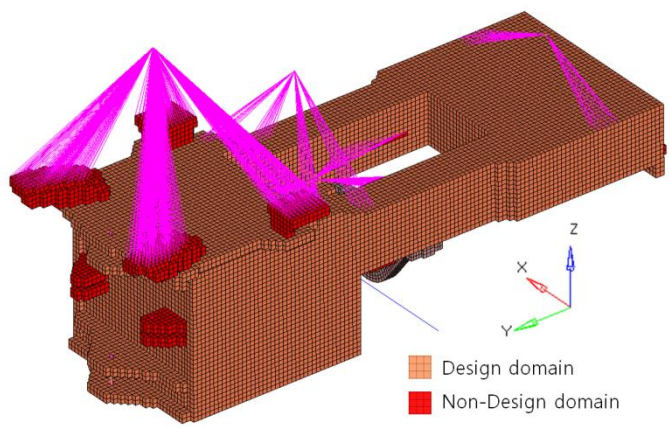

Fig. 2.2 Finite element model of a wheel load frame

Design domain of the topology optimization corresponds to the orange-colored region and non-design domain is red-colored in the finite element model in Fig. 2.2. Room for engine and transmission is removed from the design domain. Note that layouts of the main components including steering cylinders are maintained during the optimization process because they are not the scope of this study. The finite element model setup has been made using *Altair HyperMesh 12*, and *Altair OptiStruct 12*, is utilized for the

topology optimization. The whole domain is composed of 80,120 CHEXA elements [36] and 93,320 nodes and material properties are given below.

- Young's Modulus: 2.1×10^{5}
- Poisson's ration: 0.3
- Density: 7.8×10^{-9}

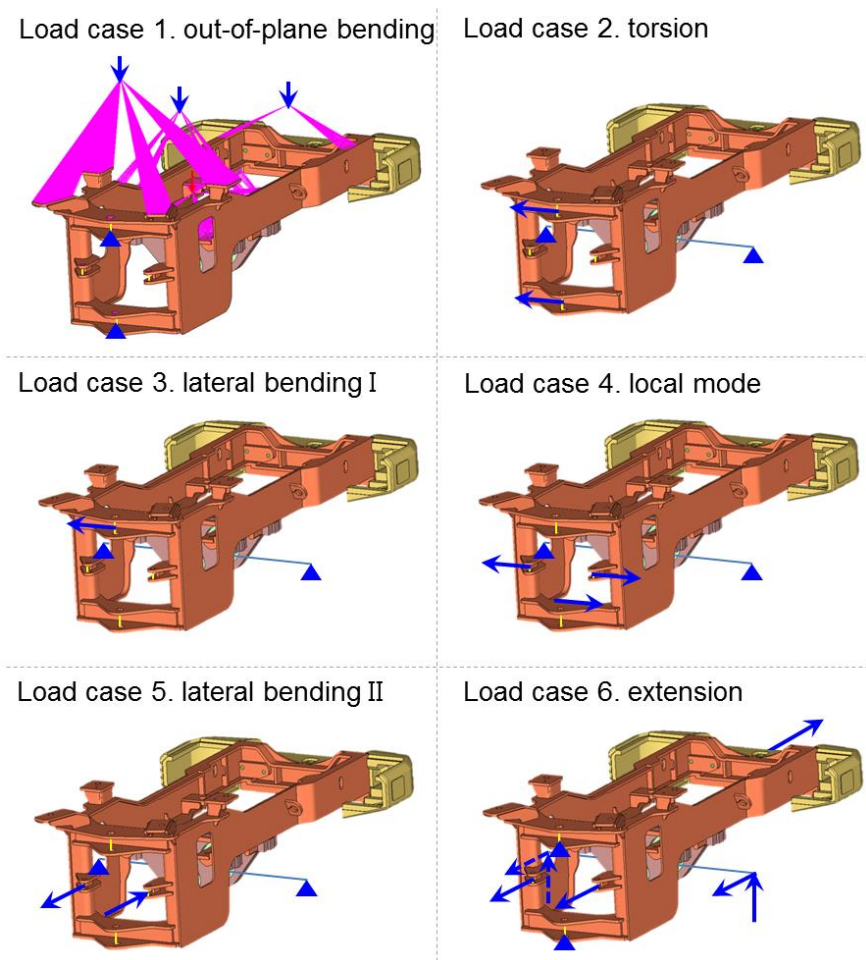

Fig. 2.3 Summary of static load conditions

2.3 Standard topology optimization of a wheel loader frame

2.3.1 Topology optimization formulation

Topology optimization is carried out using the finite element model depicted in Fig. 2.2. In this work, the SIMP (Solid Isotropic Material with Penalization) method [1-4] is employed throughout the study. The scope of the topology optimization is to find the optimum material distribution in a structure. To achieve this, the relative element-based material density which is allowed to vary continuously during the optimization process is introduced as the design variables in the SIMP method as

$$E_j(\rho_j) = \rho_j^p E_0 \quad (j = 1, 2, ..., N_e), \tag{2.1}$$

where ρ_j ($\rho_{\min} \le \rho_j \le 1$) is the density design variable of the j-th continuum element, E_0 is the nominal value of E when $\rho_j = 1$ and p is the penalty factor.

In the topology optimization with *Optistruct*, specific parameters setup is listed in the following. Other parameter values are remained as *OptiStruct* default [36] throughout this chapter.

- SIMP penalty parameter: 3
- Minimum member size control: three times of the average element size
- Symmetry constraint in the *x*-direction

The structural topology optimization with modal frequency constraints can be formulated

using two kinds of optimization problems: one is to minimize the combined compliance index [36] with the constraint functions of volume fraction and 1st eigenfrequency. The combined compliance index means the scalar sum of static compliances and reciprocal eigenvalues as in Eqs. (2.2) and (2.3). The other is to minimize the sum of static compliances with constraints of volume fraction and 1st ~ 3rd eigenfrequncies as in Eqs. (2.4) and (2.5):

$$\underset{\boldsymbol{\rho}\in\mathbf{R}^{N_e}}{\text{Minimize}} \quad \frac{1}{2}\sum_{i=1}^{6}\mathbf{f}_i^{\,T}\mathbf{u}_i + NORM\sum_{j=1}^{3}\frac{1}{\lambda_j} \tag{2.2}$$

$$\text{subject to} \quad \sum_{j=1}^{N_e}\rho_j V_j / V_s^* \le 1, \quad f_1 \ge f_1^* \tag{2.3}$$

or

$$\underset{\boldsymbol{\rho}\in\mathbf{R}^{N_e}}{\text{Minimize}} \quad \frac{1}{2}\sum_{i=1}^{6}\mathbf{f}_i^{\,T}\mathbf{u}_i \tag{2.4}$$

$$\text{subject to} \quad \sum_{j=1}^{N_e}\rho_j V_j / V_s^* \le 1, \quad f_j \ge f_j^* \ (i=1,2,3) \tag{2.5}$$

In the above equation, λ_j is the $j-$th eigenvalue, V^* denotes volume constraint, f_j^* represents the lower bound of $j-$th eigenfrequency constraint, and *NORM* is a scaling factor to calibrate the numerical order between compliance and reciprocal eigenvalue calculated at initial iteration. The value of f_j^* is the same as those of the current frame.

2.3.2 Numerical results and discussion

The topology optimization results by Eqs. (2.2)~(2.5) are shown in Fig. 2.3, where design variables above $\rho_j = 0.3$ are displayed. Modal frequencies in the case of minimizing combined compliance index as shown in Fig. 2.3(a) are higher than those in Fig. 2.3(b). This is due to the objective function as combined compliance index in which it is included to maximize the fundamental eigenfrequencies.

Notice that the truss structures, typical results of the standard topology optimization, are appeared. These kind of topological layouts are hardly possible to interpret to the welded structures which are mainly composed of relatively thin plates. One can get some information where to reinforce or not from the results in Fig. 2.4, but that's not sufficient because we cannot decide where to start the specific plate section and where to end. Moreover, it is impossible to realize X-shape cross member by means of the welding. Thus, weld manufacturability is the critical issue in the topology optimization for the construction equipment frame.

It is worth to discuss another issue in the topology optimization results illustrated in Fig. 2.5, which represent the steering cylinder dependent structure. In a wheel loader, steering mechanism is operated using embedded hydraulic cylinders which transmit the steering forces to the frame.

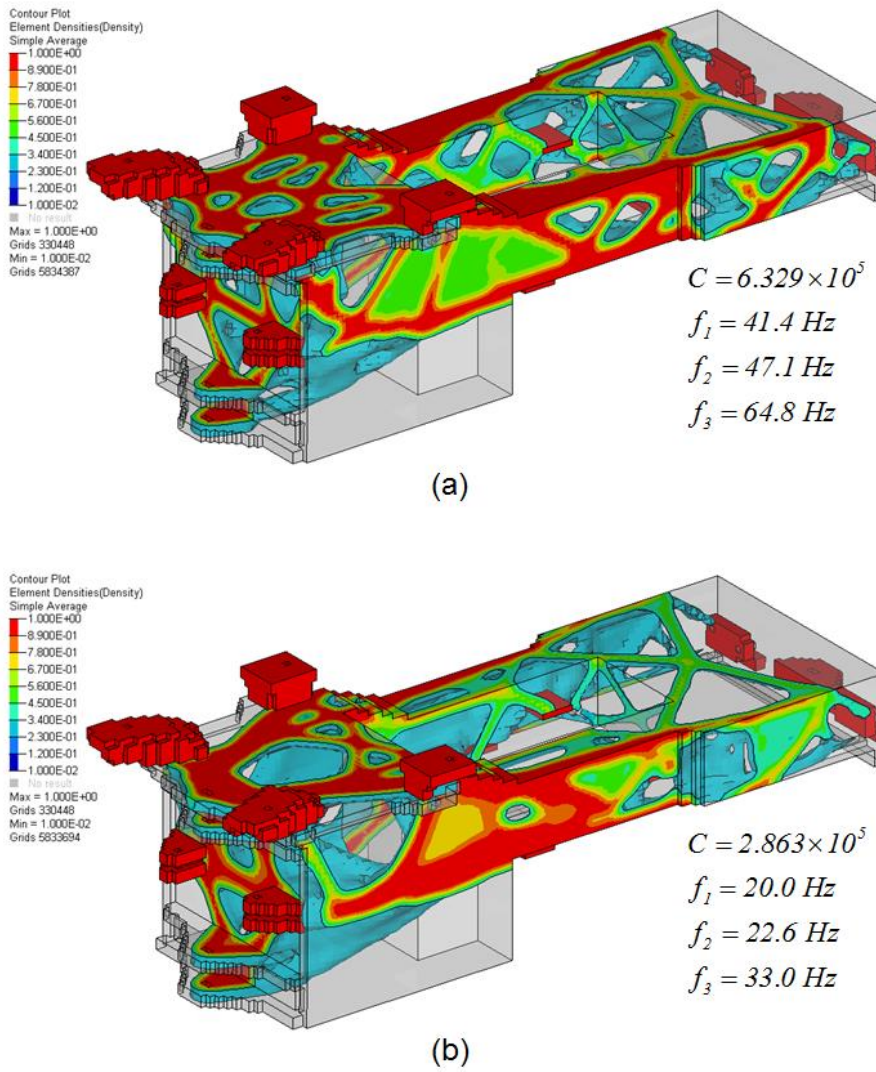

Fig. 2.4 Standard topology optimization results of a wheel loader frame (a) minimizing combined compliance index, and (b) minimizing compliance with modal frequency constraints.

In the structural point of view, the location of the steering cylinder acts as a loading point to the frame and that is why the load path is generated along the steering cylinder mounting bracket. From this result, there can be chances to optimize the cylinder location. In fact, there is some freedom in the early conceptual design stage to adjust the actuator layout for the structural performance or the manufacturing cost. The location of the actuator can be determined clearly in the simple structure. But, as complex as the structure becomes, the location of the cylinder may not be determined by the engineering intuition. Therefore, systematic design process for the determination of topological layout of the frame structure and actuator mounting location is important.

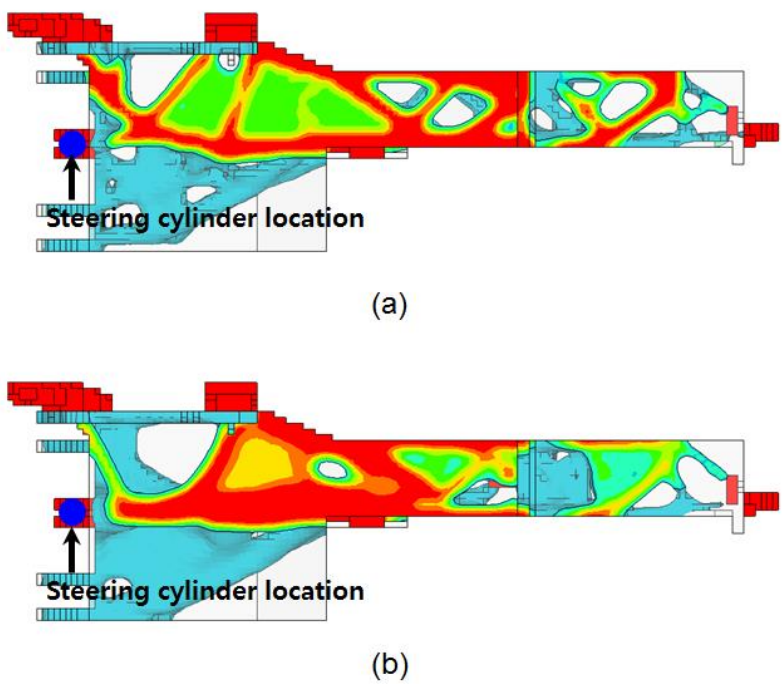

Fig. 2.5 Steering cylinder dependent structure of a wheel loader frame in side view (a) for the case of Fig. 2.4(a), and for the case of Fig. 2.4(b).

2.4 Design issues and feasibility study

2.4.1 Design issues related to topology optimization for a wheel loader frame

Figure 2.6 shows the structural design of two different types of wheel loader frames. From the design benchmarking, one can also find the major design issues for the wheel loader frame as following:

- **How can determine the location of steering cylinder and layouts of frame structure simultaneously?**
- **What is the optimal section design of the side member?**

The first question corresponds to the simultaneous design of the loading point and structural topology, while the second one is about manufacturing aspect in the topology optimization. Until now, there has been little works about the former issue; a feasibility study is followed in the following section.

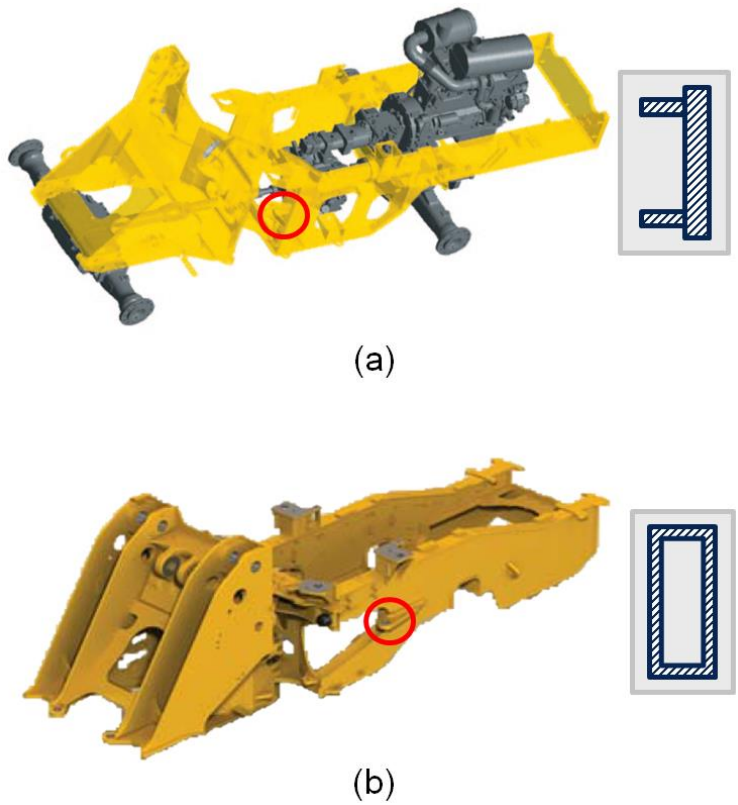

Fig. 2.6 Design of different types of wheel loader frames (a) for the case of front steering cylinder and plate-type side member [37], and (b) for the case of side inner steering cylinder and box-type side member [38].

2.4.2 Feasibility study of structural topology optimization considering loading location

Figure 2.7 demonstrate the results of the topology optimization of a wheel loader frame when the location of the steering cylinder bracket is modified to move 600mm backward ($-y$ direction) compared to the finite element model in the Fig. 2.2. Optimization setup and parameters are the same as the case in section 2.3.1 except the actuator position. The results, displayed in Fig. 2.4 and Fig 2.7, clearly show that the compliance values are improved by 7% in average. Additionally, the structural layouts in the front area of the frame appear to be more simple and efficient. From this simple numerical test, the feasibility of the simultaneous optimization between a loading point and structural topology can be assured.

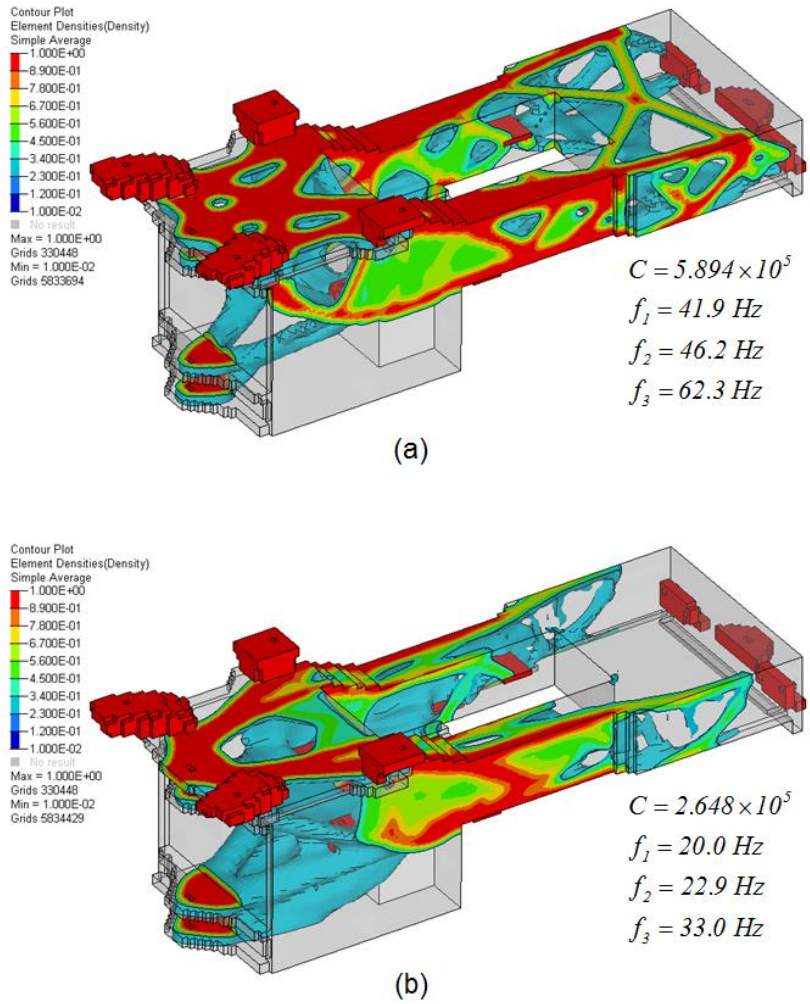

Fig. 2.7 Standard topology optimization results of a wheel loader frame with modified steering cylinder position (a) for minimizing combined compliance index, and (b) for minimizing compliance with eigenfrequency constraints.

Chapter 3.

Simultaneous optimization of a loading location and structural topology

3.1 Chapter overview

In this chapter, as schematically illustrated in Fig. 3.1, a simultaneous optimization method to determine a loading location and structural topological layout for compliance minimization under a more general movable load condition is proposed; while the magnitude and direction of an applied load is fixed, the location of an applied load is allowed to move anywhere inside the design domain or along its domain boundary. To be able to solve this type of problems, a new method will be developed and tested in this study.

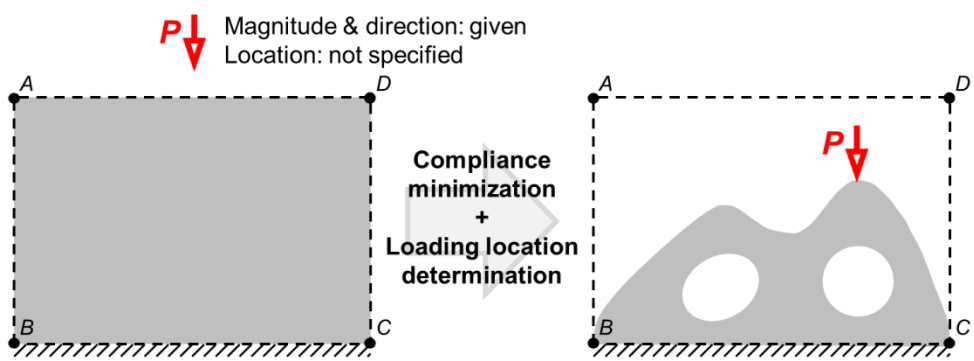

Fig. 3.1 Schematic representation of simultaneous optimization of the structural topology and loading location

One of the main issues in this study is the modeling of a load that can freely move to any point in a designated region. A new proposition is to introduce two conceptually-different design domains, one to determine the optimal loading point and the other to determine the optimal structural layout. The structural compliance as a whole will be used as a performance measure in the topology optimization setup. While the design domains are conceptually different, they share the same nodes so that the applied load is correctly transmitted to a structural layout to be optimized. Because the applied load is allowed to move, the correct load transmission requires a special attention. So, a new modeling technique is developed in this study where spring elements are used to discretize the domain for determining the loading location and continuum elements, to discretize the domain for determining the structural layout. By using the two-design domain method, it is convenient to move the applied load anywhere in the design domain without generating unwanted moment resultants, which may be otherwise difficult to suppress. The detailed explanations on this issue will be given in the next section.

Another issue is related to solution convergence. It is related to the different characteristics of the design variables, density and spring stiffness. The different contributions to the structural compliance of the spring and continuum elements also could make stable solution convergence difficult. Therefore, a multi-objective formulation with the objective functions in logarithm form is proposed for stable solution convergence.

This chapter is organized as follows. In the following section, the modeling technique

and the analysis method dealing with the movable load condition will be developed. Section 3.3 presents the optimization formulation to perform the simultaneous optimization of an optimal structural layout and loading location. Numerical case studies, including a simplified version of a wheel loader frame design problem, are presented in the next section and concluding remarks are then followed.

3.2 Modeling and analysis

3.2.1 Two design domain-based modeling technique

For the simultaneous optimization of a structural layout and loading location, the concept of two conceptually-different design domains is introduced, one for the determination of the loading location and the other for the determination of the optimal structural layout. In this approach, the problem to determine the optimal loading location is converted to a problem to connect a load initially at an arbitrary location to a node of the optimal loading location inside a domain as illustrated in Fig. 3.2. The design domain Ω^l (which will be referred to as the loading domain) in Fig. 3.2(a) is a domain introduced to determine the load location; it is used to find the single connectivity between the applied load assigned at an arbitrary location and a node of the optimal loading location inside Ω^l. The design domain Ω^s (which will be referred to as the structural domain) is a domain used to find an optimal structural layout. Although the coordinates of the nodes used to discretize the two design domains are exactly the same, the two-different design domain concept is intentionally introduced. To present the proposed modeling approach

clearly, suppose that the loading case in which a vertical load of a given magnitude is applied to a design domain, i.e., $\mathbf{P}=(0,P)$.

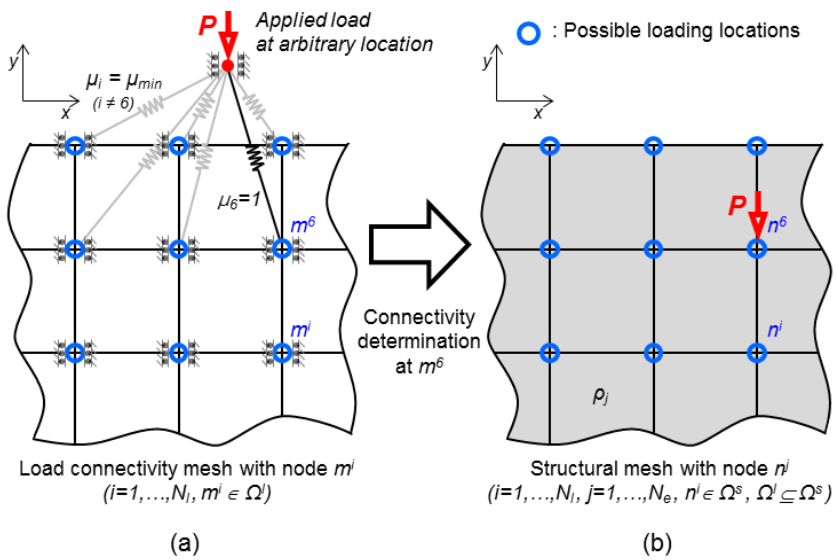

Fig. 3.2 The proposed two-domain modeling: (a) Discretized loading design domain by spring elements connecting the applied load, and (b) discretized structural design domain.

As illustrated in Fig. 3.2(a), the symbol m^i is the i-th node representing one of possible loading locations in Ω^l. The total number of possible loading locations is denoted by N_l. On the other hand, Fig. 3.2(b) shows the structural domain Ω^s discretized by quadrilateral elements. The symbol n^i is the i-th node in Ω^s and N_s denotes the total number of nodes. In dealing with Ω^s, however, it will be more convenient to use N_e to denote the total number of elements because the density-based topology optimization will be used for the structural part. Note that the coordinates of

node m^i are set to be the same as those of n^i because Ω^l is always a subset of Ω^s ($\Omega^l \subseteq \Omega^s$). With this setting, it is straightforward to transmit the applied load applied at m^i directly to n^i of the structural design domain. Although two design domains are used for conceptual convenience, the actual loading location moves freely around in the design domain.

For streamlined determination of the optimal loading location, it is assumed at the beginning of optimization iterations that all m^i's are connected to the applied load **P** of a given magnitude and direction through spring elements. At the initial state of the simultaneous optimization, the load can be located at any arbitrary position but it is easier to locate it outside the domain Ω^s without loss of generality. Only six spring connections are sketched in Fig. 3.2(a) for clear illustration of the spring element connections in Ω^l. The connection from the load to m^i is controlled by the value of its spring stiffness (k_i) which is interpolated as

$$k_i(\mu_i) = \mu_i^{\eta} k_0 \quad (i = 1, 2, ... N_l), \tag{3.1}$$

where μ_i ($\mu_{\min} \le \mu_i \le 1$) is the design variable assigned to the i-th connecting spring element and η is the penalty parameter. The nominal spring stiffness is denoted by k_0, the value of which will be discussed in section 3.4. The notion of the spring elements to represent connectivity was used for different purposes in some earlier topology optimization problems [10, 21].

A special attention is needed in order to correctly transfer the applied load **P** to any node

(m^i). This means that the loading direction should not be changed and also no additional resultant, in particular, the moment resultant, should be produced by improper load transfer. To fulfill these requirements, the following approach is developed.

First, the stiffness of the i-th spring element is defined as

$$\mathbf{k}^i = (k_x^i, k_y^i)^T = (0, k_i(\mu_i))^T, \tag{3.2}$$

where k_x and k_y is the x- and y-directional stiffness, respectively. For the problem in consideration, $k_x = 0$ is imposed because the load is applied along the vertical direction, i.e., the y-direction. (If the load is applied along the x-direction, $\mathbf{k}^i = (k_i(\mu_i), 0)^T$ will be used.) Conceptually, this modeling technique is equivalent to use roller supports at m^i. If k_x is not set to be zero, the load transferred to node m^i could produce any other load such as a nonzero moment applied at any node.

Next, the displacements of nodes m^i and n^i occupying the same coordinates must be coupled to transfer the applied load specified in Ω^l to a structure defined in Ω^s. Specifically, the following conditions will be

$$u_y^{m^i} = u_y^{n^i} \quad (i = 1, 2, ..., N_l). \tag{3.3}$$

To address the importance of the three above-mentioned technique, the connectivity models without and with the proposed techniques are illustrated in Fig. 3.3(a) and Fig. 3.3(b), respectively. In the illustration, the applied load **P** is assumed to be connected to

m^6 which is coupled with n^6. (Here, the value of $\mu_i = 1$ implies the state of connection and the value of $\mu_i = \mu_{\min}$, the state of disconnection.) The model in Fig. 3.3(a) not imposing $k_x^i = 0$ and $u_y^{m^i} = u_y^{n^i}$ will generate an additional resultants, which should not be applied to the structure; only the vertical force should be non-vanishing. If the proposed techniques as described in Fig. 3.3(b) are used, only the vertical force is correctly transmitted to the structure to be optimized. Although only the vertical loading case is considered as an illustration, the proposed techniques can be extended for any load type.

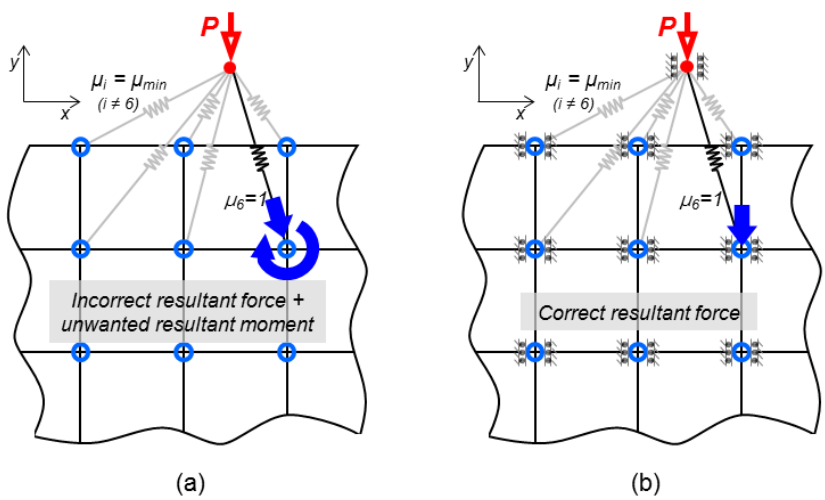

Fig. 3.3 Illustration of load transferring issue: (a) Erroneous generation of the resultant if the load is directly connected to the nodes of the load domain, and (b) correct transfer of the applied load to the nodes of the load domain and thus to the nodes of the structural domain .

Regarding the topology optimization modeling for the structural part defined in Ω^s, the standard density-based approach [1] is used. Thus, Young's modulus of continuum element j in Fig. 3.2(b) is interpolated as

$$E_j(\rho_j) = \rho_j^p E_0 \quad (j = 1, 2, ..., N_e), \tag{3.4}$$

where ρ_j $(\rho_{\min} \le \rho_j \le 1)$ is the density design variable of the j-th continuum element, E_0 is the nominal value of E when $\rho_j = 1$ and p is the penalty factor.

3.2.2 Finite element formulation for the two design domain-based model

Since the construction of the finite element system equation is well established, the finite element equation is simply given below without any detailed derivation:

$$\mathbf{F} = \mathbf{K}\mathbf{u} = (\mathbf{K}_l + \mathbf{K}_s)\mathbf{u}, \tag{3.5}$$

where $\mathbf{F}$ is the global force vector. The global nodal displacement vector $\mathbf{u}$ is defined as $\mathbf{u} = \{\mathbf{u}_l \ \mathbf{u}_s\}^T$ where $\mathbf{u}_l$ and $\mathbf{u}_s$ are the nodal displacement vectors defined in Ω^l and Ω^s, respectively. The global stiffness matrix $\mathbf{K}$ consists of two system matrices $\mathbf{K}_l$ and $\mathbf{K}_s$ resulting from the discretization of Ω^l and Ω^s:

$$\mathbf{K} = \mathbf{K}_l + \mathbf{K}_s = \mathop{\mathbf{A}}_{i=1}^{N_l} \mathbf{k}^i + \mathop{\mathbf{A}}_{j=1}^{N_e} \mathbf{k}_s^j, \tag{3.6}$$

where $\mathbf{k}^i$ and $\mathbf{k}_s^j$ denote the i-th spring and j-th continuum element stiffness matrices, respectively. For the case of vertical applied load (the y-directional load), the expression of $\mathbf{k}^i$ is the same as Eq. (3.2). In Eq. (3.6), $\mathbf{A}$ denotes the element assembly operator. If the condition given by (3.3) is written in matrix form,

$$\mathbf{Cu} = \mathbf{0}, \tag{3.7}$$

If the Lagrange multiplier $\boldsymbol{\xi}$ is introduced to handle (3.7), equations (3.5) and (3.7) can be put into the following form:

$$\begin{bmatrix} \mathbf{K} & \mathbf{C}^T \\ \mathbf{C} & \mathbf{0} \end{bmatrix} \begin{Bmatrix} \mathbf{u} \\ \boldsymbol{\xi} \end{Bmatrix} = \begin{Bmatrix} \mathbf{F} \\ \mathbf{0} \end{Bmatrix}. \tag{3.8}$$

A few remarks regarding the size of the system matrix may be made. In most of practical engineering problems, the domain size of Ω^l is much smaller than Ω^s because the candidate loading points are usually limited. Therefore, the increase in the degrees of freedom in (3.8) is marginal. On the other hand, the use of (3.8) based on the two conceptual design domains facilitates the control of the convergence in the topology optimization problem as shall be seen later with numerical case studies.

3.3 Topology optimization formulation

Based on the two conceptual design domain method presented in the previous section, the following multi-objective formulation is proposed for the simultaneous optimization:

$$\underset{\boldsymbol{\mu}\in\mathbf{R}^{N_l},\,\boldsymbol{\rho}\in\mathbf{R}^{N_e}}{\text{Minimize}} \quad \Psi(\boldsymbol{\mu},\boldsymbol{\rho}) = \ln\left[\left\{C_l(\boldsymbol{\mu},\boldsymbol{\rho})+1\right\}\left\{C_s(\boldsymbol{\mu},\boldsymbol{\rho})+1\right\}\right] = \ln\left(C_l+1\right)+\ln\left(C_s+1\right) \tag{3.9}$$

$$\text{subject to} \qquad V(\boldsymbol{\rho}) = \sum_{j=1}^{N_e} \rho_j V_j / V_s^* \le 1, \tag{3.10}$$

$$S(\boldsymbol{\mu}) = \sum_{i=1}^{N_l} \mu_i \le 1, \tag{3.11}$$

$$Q(\boldsymbol{\mu}) = \sum_{i=1}^{N_l} \mu_i (1-\mu_i) \le \delta \,, \tag{3.12}$$

$$\begin{aligned} &\mu_{\min} \le \mu_i \le \mu_{\max} = 1 \qquad (i = 1,2,\cdots,N_l) \\ &\rho_{\min} \le \rho_j \le \rho_{\max} = 1 \qquad (j = 1,2,\cdots,N_e) \end{aligned} \tag{3.13}$$

with $\boldsymbol{\rho} = \{\rho_1, \rho_2, \cdots, \rho_{N_e}\}^T$ and $\boldsymbol{\mu} = \{\mu_1, \mu_2, \cdots, \mu_{N_l}\}^T$.

In Eq. (3.9), C_l and C_s denote the compliances of the discretized spring and continuum element systems defined in Ω^l and Ω^s, respectively. They are defined as

$$C_l(\boldsymbol{\mu}, \boldsymbol{\rho}) = \frac{1}{2} \mathbf{u}_l^T(\boldsymbol{\mu}, \boldsymbol{\rho}) \mathbf{K}_l(\boldsymbol{\mu}) \mathbf{u}_l(\boldsymbol{\mu}, \boldsymbol{\rho}) \,, \tag{3.14}$$

$$C_s(\boldsymbol{\mu}, \boldsymbol{\rho}) = \frac{1}{2} \mathbf{u}_s^T(\boldsymbol{\mu}, \boldsymbol{\rho}) \mathbf{K}_s(\boldsymbol{\rho}) \mathbf{u}_s(\boldsymbol{\mu}, \boldsymbol{\rho}) \,. \tag{3.15}$$

Now, the role of each function defined in (3.14) and (3.15) will be examined. First, the objective function Ψ consists of the product of C_l and C_s because its minimization is equivalent to the maximization of the structural stiffness. The minimization of C_l helps push the design variables μ_i $(i = 1,\cdots,N_l)$ towards their lower ($\mu_{\min}$) and upper ($\mu_{\max} = 1$) bounds although explicit penalty functions will be also introduced as Eq. (3.12).

The logarithm form of the product of C_l and C_s in the definition of Ψ is employed to adjust a balance between C_l and C_s because the sizes of Ω^l and Ω^s are different and the number of the candidate loading points in Ω^l can vary depending on problems. Also, due to the coupling between different types of optimizations, the determinations of

the loading location and optimal topological structural layout, a balance between the sensitivities of C_l and C_s should be made. As the effectiveness of the logarithmic form of a product of two functions was demonstrated by Kim and Kim [39] for a similar issue, the logarithmic form of the objective function given in Eq. (3.9) is used. More discussions on this form will be given later.

The constraint function Eq. (3.10) is simply the statement of a volume constraint where V_j and V^* denote the volume of the j-th continuum finite element and the allowed total volume. Equations (3.11) and (3.12) altogether ensure that the applied load be connected to a single node in Ω^l. The reason to use two constraint functions (3.11) and (3.12) is that the success of the present simultaneous optimization heavily depends on the state of the single connection between the applied load and a node in Ω^l. Because optimal structural layouts depend critically on the applied load, the correct transfer of the load to the structure is critical. For instance, if the load is connected to multiple nodes even with small values of μ_i, the obtained layout could be quite different from the true optimal layout. Therefore, we introduced the two conceptual domain method to ensure that the applied load is transmitted to a single point in the structure. Instead of Eq. (3.11), following form may be considered as an alternative: $S(\boldsymbol{\mu}) = \sum_{i=1}^{N_l} \mu_i \le 1 + \mu_{\min} \times (N_l - 1)$.

Although compliance in the load domain C_l plays the role to push μ_i towards either $\mu_{\min}$ or $\mu_{\max}$, the explicit penalty function Q controls the convergence speed of the load

design variable μ_i. It makes possible to success the simultaneous optimization if the upper bound δ is selected properly. The upper bound δ in Eq. (3.12) should be zero theoretically, but the use of too small values result in pre-matured solutions. Its value should be tuned to improve solution convergence so that μ_i takes on either $\mu_{\min}$ or $\mu_{\max}$ at the optimum. Our numerical studies suggest that the values of δ ranging between 0.3 and 0.8 yield satisfactory results (All the results of the numerical studies are listed in Appendix. A1).

For the update of design variables (μ_i and ρ_j), the sensitivities of the objective function is calculated by using the adjoint method [40]:

$$\frac{\partial \Psi(\boldsymbol{\mu},\boldsymbol{\rho})}{\partial \boldsymbol{\mu}} = \frac{1}{2(C_l+1)}\mathbf{u}_l^T \frac{\partial \mathbf{K}_l(\boldsymbol{\mu})}{\partial \boldsymbol{\mu}}\mathbf{u}_l - \boldsymbol{\lambda}^T \frac{\partial \mathbf{K}_l(\boldsymbol{\mu})}{\partial \boldsymbol{\mu}}\mathbf{u}_l$$
$$\frac{\partial \Psi(\boldsymbol{\mu},\boldsymbol{\rho})}{\partial \boldsymbol{\rho}} = \frac{1}{2(C_s+1)}\mathbf{u}_s^T \frac{\partial \mathbf{K}_s(\boldsymbol{\rho})}{\partial \boldsymbol{\rho}}\mathbf{u}_s - \boldsymbol{\lambda}^T \frac{\partial \mathbf{K}_s(\boldsymbol{\rho})}{\partial \boldsymbol{\rho}}\mathbf{u}_s \tag{3.16}$$

In equation (3.16), the adjoint variable $\boldsymbol{\lambda}$ is defined as

$$\boldsymbol{\lambda} \equiv \left[\frac{\partial \Psi}{\partial \mathbf{u}}\mathbf{K}^{-1}(\boldsymbol{\mu},\boldsymbol{\rho})\right]^T = \mathbf{K}^{-1}(\boldsymbol{\mu},\boldsymbol{\rho})\left(\frac{\partial \Psi}{\partial \mathbf{u}}\right)^T$$
$$= \mathbf{K}^{-1}(\boldsymbol{\mu},\boldsymbol{\rho})\left[\frac{\mathbf{K}_l(\boldsymbol{\mu})\mathbf{u}_l(\boldsymbol{\mu},\boldsymbol{\rho})}{C_l(\boldsymbol{\mu},\boldsymbol{\rho})+1} + \frac{\mathbf{K}_s(\boldsymbol{\rho})\mathbf{u}_s(\boldsymbol{\mu},\boldsymbol{\rho})}{C_s(\boldsymbol{\mu},\boldsymbol{\rho})+1}\right]. \tag{3.17}$$

As remarked earlier, the proposed form of the objective function has an adaptive scaling effect in the sensitivity calculation at every iteration. If the compliance C_l becomes larger, sensitivities the objective function in Eq. (3.9) gets less sensitive to the variations

of the C_l because of the normalization factor C_l in the denominator of Eq. (3.17), and vice versa.

3.4 Numerical examples

In this section, numerical examples will be considered to show the validity and effectiveness of the proposed method. Several case studies having different conditions on the allowed range of the location of the applied load are considered.

In Case 1, the load is allowed only along the direction of the applied load – this recovers the problem solved in Fuchs and Moses [26]. Case 2 deals with the problem where the applied vertical load can move along the upper boundary of the design domain. So the moving path is perpendicular to the loading direction – a similar problem was solved in [31]. Moreover, the case when the applied load can move around in a designated two-dimensional domain is considered in case study 3. The specific problem motivated by an actual industrial application is the simultaneous optimization of the structural topology and the actuator loading position for a simplified wheel loader frame - this is a new type of problems, not solved or considered earlier. Finally, extension to movable load examples in the three-dimensional structural domain is followed.

To check if the proposed method is indeed effective, a set of standard structural topology optimization problems considering all possible loading locations for a load of a given magnitude and direction was solved and compared their best solution with the optimized

solution obtained by the proposed simultaneous optimization. To update the design variables, the method of moving asymptotes [41] is employed as the gradient based optimization algorithm. In order to avoid the checkerboard and mesh-dependent problem, a density filter technique [42] is applied with the filter radius being three times the average element size in all examples. Note that the spring elements in the loading domain are not filtered. Also the values of $\mu_{\min} = \rho_{\min} = 0.001$ for the lower bounds and $\eta = p = 3$ for the penalty parameters are used throughout the present investigation.

3.4.1 Case study 1: loading point moving along the given load direction

As the first case, consider the simultaneous design problem, in which the load is allowed only along the direction of the applied load under the volume constraint ratio $\overline{V^*} = 10\%$. Figure 3.4(a) illustrates the design domain and the line along which the applied vertical load can move. The bottom side ends are simply supported. The structural domain is discretized by 96×96 4-node plane stress elements. The thickness is taken to be 10 mm. In this case, the loading domain consists only of a vertical line which is discretized by 49 candidate nodes marked by circles in Fig. 3.4(a). The node number varies from 1 to 49 from the bottom. The material properties of the continuum elements are given by Young's modulus $E_0 = 210$ GPa and Poisson's ratio ν =0.3.

To determine the nominal value of k_0, some care must be taken. It is found through numerical tests that if the value of k_0 ranges between 10^{-1} to 10^{-4} times smaller than the

diagonal stiffness of the continuum element; successful optimization result can be obtained because the spring element do not affect the stiffness in the continuum domain significantly (More details on the parameter study is summarized in Appendix. A1.). A similar approach was used by Buhl [24] who solved the simultaneous topology optimization of structures and supports in which the structural domain is not perturbed significantly by a proper choice of the stiffness of spring elements. The initial values of all design variables are set to be $\rho_i = \overline{V^*}$ and $\mu_i = 1/N_l$. In this problem, the upper bound value of $\delta = 0.7$ was found to yield good convergence.

Figure 3.4(b) shows the result giving the smallest value of C_s by the standard structural topology optimization. It is the best one among all results obtained for the problems under different loading locations assigned at m^i ($i = 1, \cdots, N_l = 49$). The result in Fig. 3.4(b) is the optimal layout obtained when the load is directly applied at m^{24} (corresponding the variable states of $\mu_i = \mu_{\min}$ except $\mu_{24} = \mu_{\max} = 1$). Figure 3.4(c) shows the optimized structural layout by the proposed simultaneous optimization formulation. The bold line in the middle is the link connecting the applied load and m^{24}. The comparison of Fig. 3.4(b) and Fig. 3.4(c) shows that the present formulation produces the same topological layout and identifies the optimal loading location as in Fuchs and Moses [26]. The compliance values are almost identical (3.296 vs. 3.299).

The iteration histories are plotted in Fig. 3.5. The decrease pattern of the objective function Ψ is shown in Fig. 3.5(a). It also shows intermediate structural layouts and

loading locations. At the very beginning of the optimization process, the load design variables decrease to satisfy the explicit penalty constraint in Eq. (3.14), resulting in the increase of C_l. Otherwise, the objective function is rather monotonically reduced. Figure 3.5(b) also exhibits the stable convergences of the constraint functions V, S and Q.

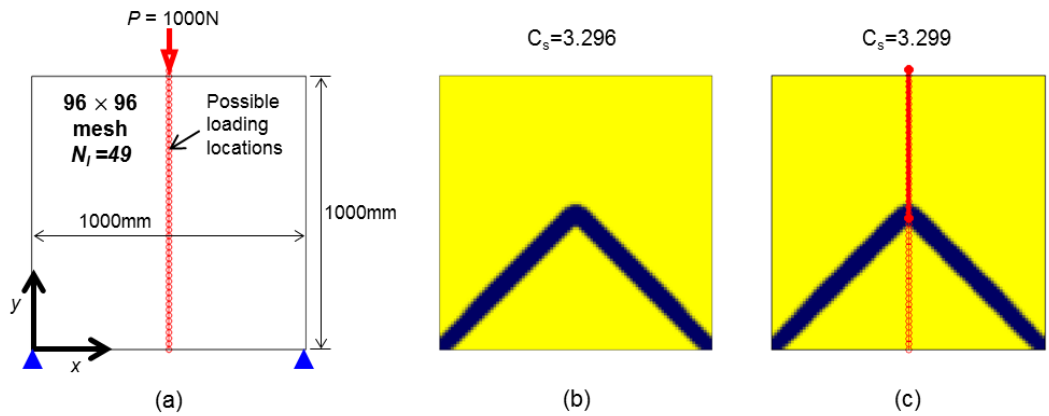

Fig. 3.4 Case study 1 for a vertically-movable load: (a) Design domain with prescribed load/boundary conditions, (b) the best result from standard structural topology optimization considering all possible loading locations, and (c) the result by the proposed simultaneous optimization method.

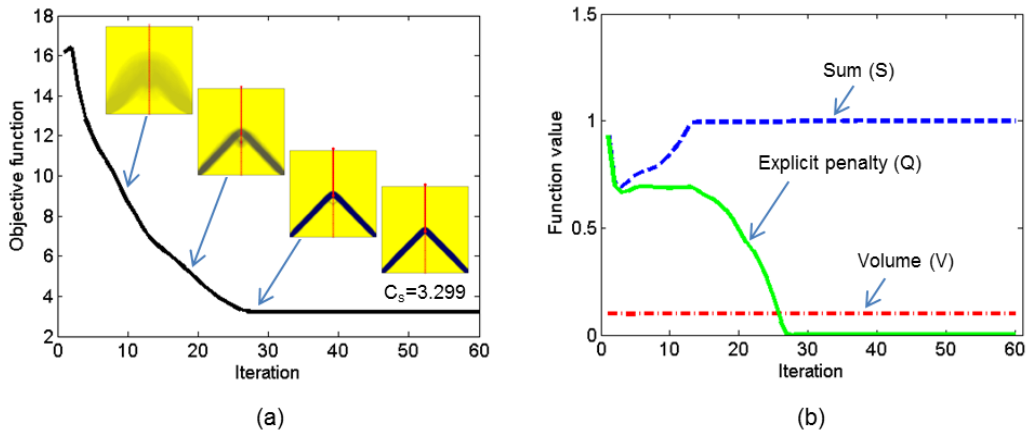

Fig. 3.5 Iteration history for case study 1: (a) The objective function with intermediate layouts, and (b) the constraint functions.

3.4.2 Case study 2: loading point moving perpendicular to the load direction

In this case, the applied load is allowed to move along the perpendicular direction to its loading direction. Two problems illustrated in Fig. 3.6(a) and Fig. 3.8(a) will be solved. The problem defined in Fig. 3.8(a) differs from that in Fig. 3.6(a); the problem depicted in Fig. 3.8(a) has a non-design domain (such as a service area of a wheel loader frame) inside the rectangular design domain.

- **Case Study 2-A**

The structural design domain given in Fig. 3.6(a) is discretized with 32×80 4-node plane stress elements (thickness 10mm). In this problem, we considered only 4 *unevenly-*

spaced candidate loading locations along the top horizontal boundary where a vertical force is applied. If the candidate loading points were evenly spaced, two central points would be optimal. Because we aim to find only one optimal loading point, we intentionally use unevenly-spaced candidate loading locations. The distances from the left side to the candidate locations are specified in Fig. 3.6(a). The material properties and optimization parameters are the same as those used in Case Study 1 except $\overline{V^*} = 30\%$.

Figure 3.6(b) shows all of the optimized structural layouts by the standard topology optimization when the load is applied at 4 different locations lying along the boundary. Obviously, the optimized layouts differ depending on the loading locations. The smallest value of C_s is found when the applied load is at m^2. The optimized result by the proposed simultaneous optimization formulation is shown in Fig. 3.6(c). It is virtually identical to the layout shown in Fig. 3.6(b) for the applied load at m^2. The iteration history plot as shown in Fig. 3.7 exhibits stable convergence behavior of the objective and constraints.

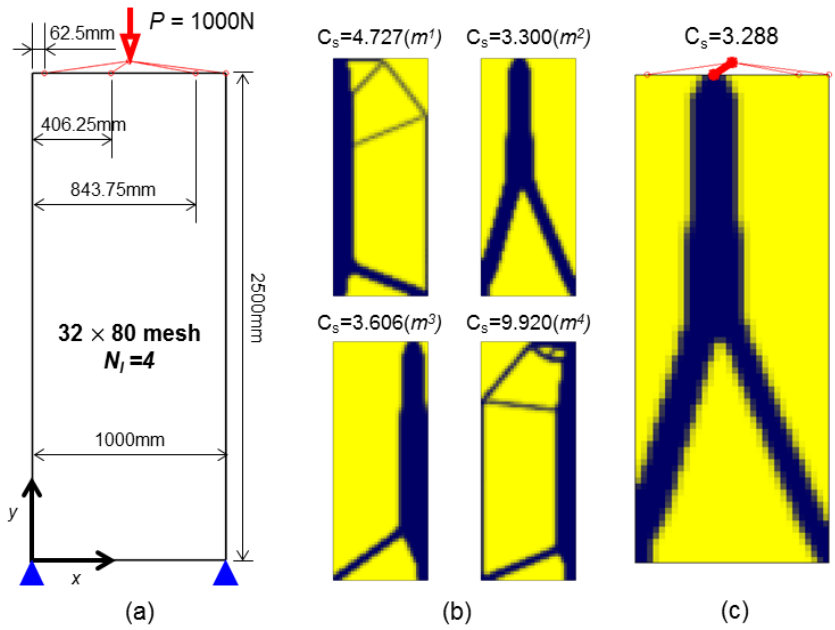

Fig. 3.6 Case study 2-A for a horizontally-movable load: (a) Design domain with prescribed load/boundary conditions, (b) All of the results from standard topology optimization considering all possible loading locations, and (c) the result by the proposed simultaneous optimization method.

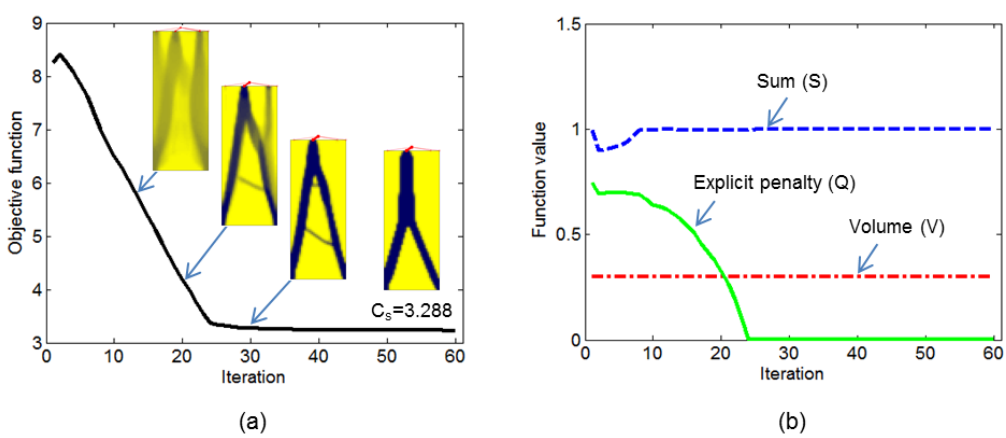

Fig. 3.7 Iteration history for case study 2-A: (a) The objective function with intermediate layouts, and (b) the constraint functions.

- **Case Study 2-B**

This problem depicted in Fig 3.8(a) deals with more realistic situations where the rectangular design domain has a non-design domain in it. The size of the non-design domain is stated in Fig. 3.8(a). In this case, 21 evenly-spaced candidate loading locations are considered along the top horizontal boundary where a vertical force is applied. The structural domain is composed of 40×100 elements. The material property and the initial values of the design variables are same as those in Case Study 1 but $\overline{V^*} = 20$ %. The value of $\delta = 0.3$ was found to yield satisfactory results for this problem.

Figure 3.8(b) shows the best solution at m^{15} among all possible optimal layouts for loads applied at all possible candidate locations. The optimized layout shown in Fig. 3.8(c) is obtained by the proposed simultaneous optimization method. The two results are almost identical. The compliance value (C_s) by the proposed method is slightly better than that by the standard structural topology optimization with a fixed load. The iteration histories in Fig. 3.9 exhibit the same convergence behavior as found in earlier problems.

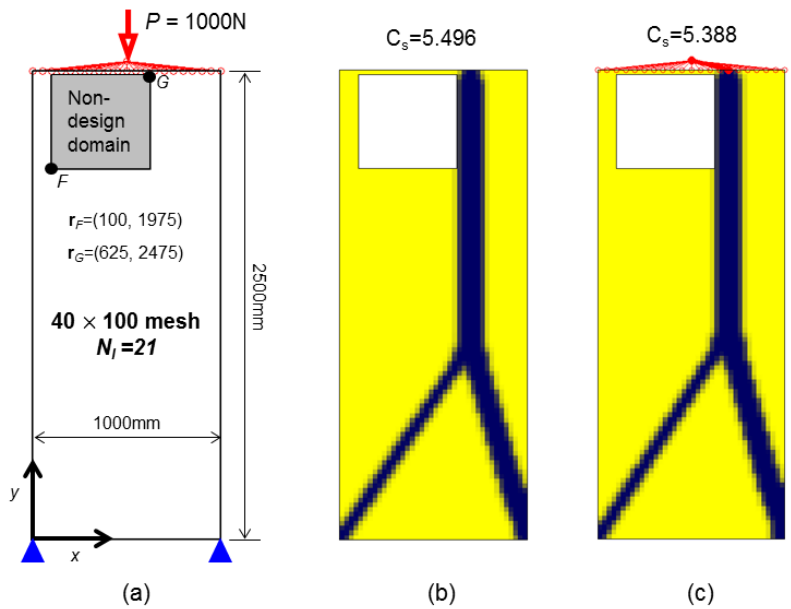

Fig. 3.8 Case study 2-B for a horizontally-movable load: (a) Design domain having a non-design domain and prescribed load/boundary conditions, (b) the best result from standard topology optimization considering all possible loading locations, and (c) the result by the proposed simultaneous optimization method.

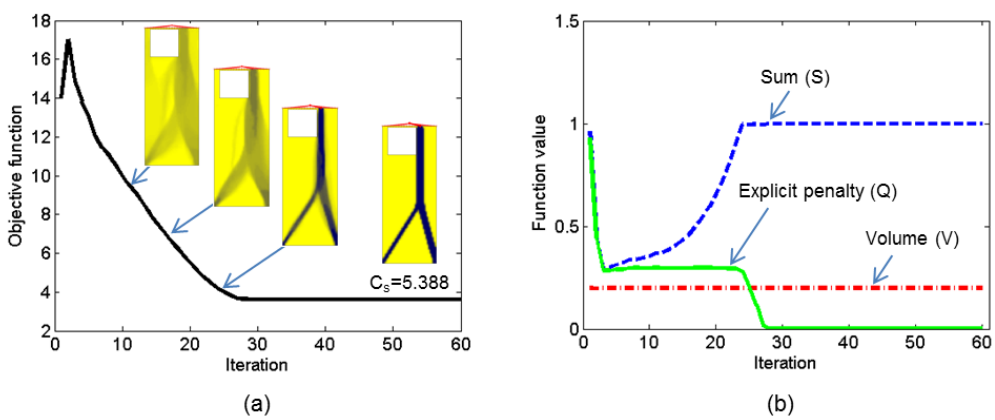

Fig. 3.9 Iteration history for case study 2-B: (a) The objective function with intermediate layouts and (b) the constraint functions.

3.4.3 Case study 3: loading point moving in a two-dimensional region

The simultaneous design problem where two multi-load cases are illustrated in Figs. 3.10 and 3.13 is considered. The design domain is a simplification of a wheel loader frame with an embedded steering actuating cylinder. Obviously, the optimal frame layout should be found. Also, the position of the steering cylinder which determines the loading location of the steering force within a frame should be determined in an early concept design stage.

- **Case Study 3-A**

The rectangular domain shown in Fig. 3.10 has a few non-design domains as in the actual design. Among the two load cases, load case 1 in Fig. 3.10(a) considers a movable steering force acting horizontally at one of the candidate loading points marked with circles. A fixed horizontal force in the rear region of the design domain is also considered as a part of load case 1. On the other hand, the load case load case 2 in Fig. 3.10(b) has workloads only. (These loads are some of the typical loads that should be considered in the frame design.) In defining the structural compliance C_s, the structural compliances under each load cases are equally weighted.

The left arrow of magnitude of $P = 2000$ N in load case 1 stands for a steering cylinder load. There are 16 candidate loading points. They are equally distanced vertically and uniformly distributed horizontally behind the rectangular non-design domain. The coordinates of some candidate points are given in Fig. 3.10(a). The volume constraint

ratio is $\overline{V}^{*} = 30\%$. The bound value of $\delta = 0.3$ for (3.14) was found to be suitable. Material properties and other parameters are the same as in the previous problems.

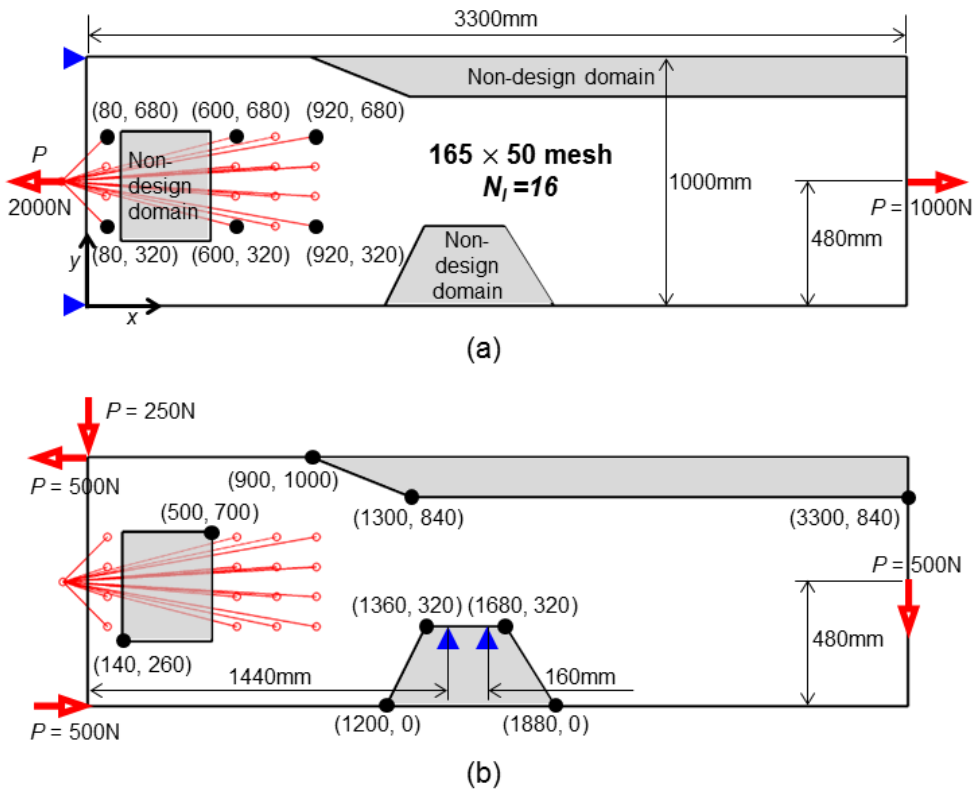

Fig. 3.10 Case study 3-A for a movable load in a given two-dimensional region: (a) Load case 1 consisting of the horizontal movable load **P** with a non-movable load and (b) load case 2 consisting of non-movable workloads only.

Figure 3.11(a) shows the best result among all results obtained by the standard structural topology optimization for loads separately applied at all of the candidate locations. So, 16 structural topology optimization cases must be solved. All of these 16 results can be seen in the Appendix. A2. The optimized result by the proposed simultaneous optimization of the structural layout and loading location is shown in Fig. 3.11(b). The topological layouts between the two results are not 100% identical, but the topologies of the main load-carrying members are almost the same. Also, the values of C_s by the two results are sufficiently close to each other.

While the result in Fig. 3.11(a) requires 16 topology optimization runs, the present formulation yielded the result by one optimization run. To find the optimal loading location and corresponding structural topology, total CPU time increases proportional to the number of the candidate loading locations in case of the standard topology optimization with pre-determined loads. On the other hand, the proposed simultaneous design method can optimize the loading location and structural topology at the same time. Its CPU time does little depend on the number of the candidate loading points. To show the effectiveness of the simultaneous design, total CPU time for the optimization is compared in the following.

- Standard topology optimization with 16 pre-determined load cases: *13,132 sec*
- Proposed simultaneous optimization: *1,664 sec*

Although proposed simultaneous optimization requires parameter tuning, for example, k_0 in Eq. (3.1) and δ in Eq. (3.12), sufficient efficiency can be assured. According to

the parameter studies in Appendix. A.1, the range of tuning parameter is relatively small.

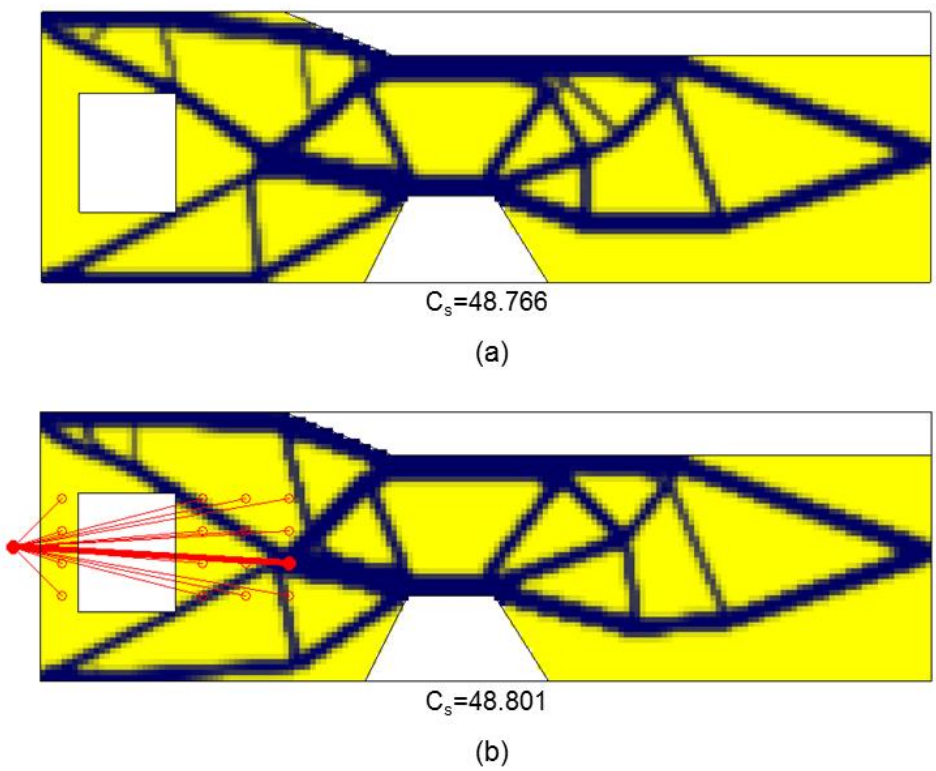

Fig. 3.11 The optimized layouts for case study 3-A: (a) The best result from standard structural topology optimization considering all possible loading locations, and (b) the result by the proposed simultaneous optimization method.

The iteration histories and intermediate layouts during optimization iterations are shown Fig. 3.12(a). The values of the constraint functions shown in Fig. 3.12(b) converge to the target values stably.

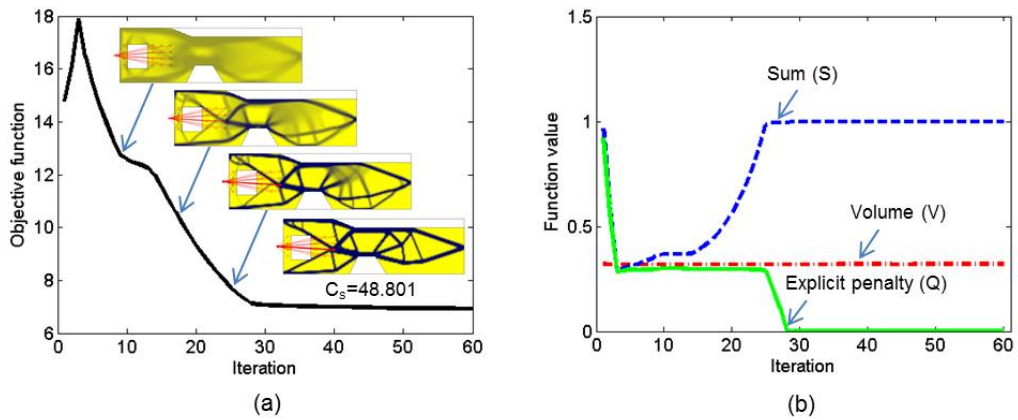

Fig. 3.12 Iteration history for case study 3-A: (a) The objective function, and (b) the constraint functions.

- **Case Study 3-B**

In this case, the simultaneous optimization with three load cases is demonstrated. There is horizontal cylinder load similar to the previous case study as shown in Fig. 3.13(a), vertical cylinder load in Fig. 3.13(b) and workloads in Fig. 3.13(c). The size of the structural design domain and the support locations are the same as the case study 3-A in Fig. 3.10, unless otherwise specified in Fig. 3.13. Weighting factors of the each load cases are equals to one for the compliance calculation. There are 25 possible loading locations equally spaced. Material properties and optimization parameters are the exactly same with the case study 3-A.

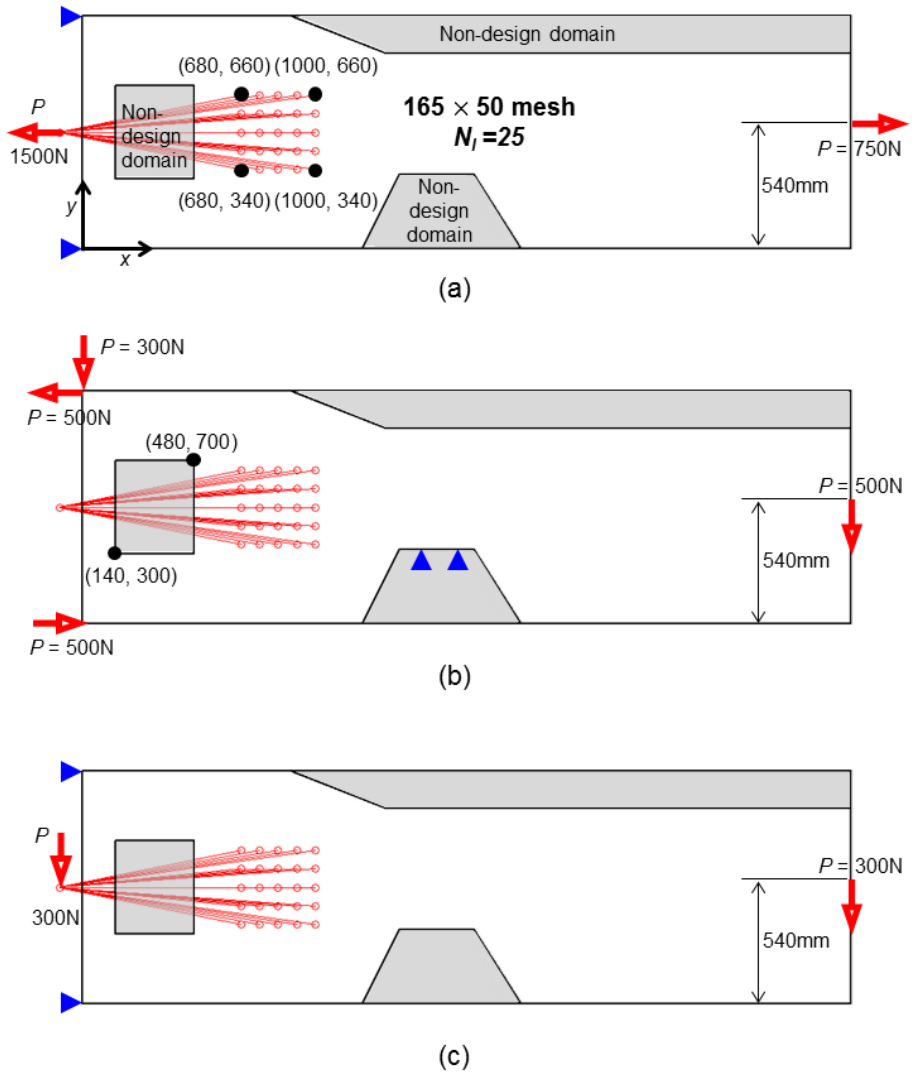

Fig. 3.13 Case study 3-B for a movable load in a given two-dimensional region: (a) Load case 1 consisting of the horizontal movable load **P** with a non-movable load, (b) load case 2 consisting of the vertical movable load **P** with a non-movable load and, (c) load case 3 consisting of non-movable workloads only.

Figure 3.14(a) depicts the simultaneous optimization result for the example shown in Fig. 3.13. If we discretize the load domain more with 81 candidate loading points, almost same results can be obtained as displayed in Fig. 3.11(b); the determined loading point is in the same location and topological layouts in the structural domain also almost identical. These results show the effectiveness of the developed simultaneous optimization method. Although the load domain is discretized with more candidate loading points, consistent solution can be obtained. Notice that the optimal loading location is determined at the point in the upper right corner in the load domain. One may expect the optimal loading location could be determined at the point in the lower right corner close to the support point. But, the loading point determination under complex conditions, such as multiple load and complex geometry, is very difficult to find with the engineering intuition. In this situation, the proposed method can be utilized efficiently.

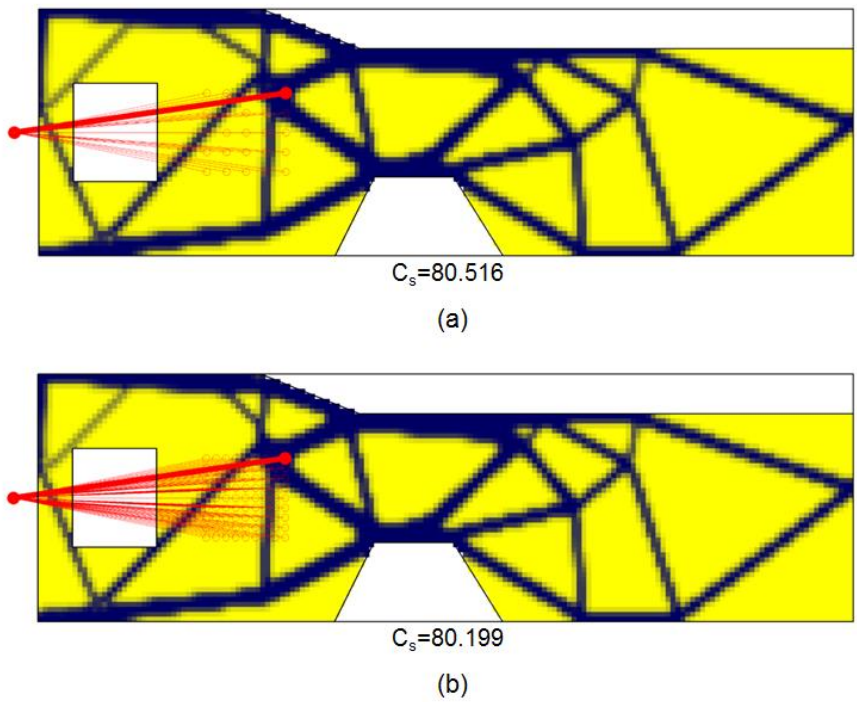

Fig. 3.14 The optimized layouts for case study 3-B using the proposed simultaneous optimization method with (a) 25 candidate loading points, and (b) with 81 candidate loading points.

3.4.4 Case study 4: 3-dimensional examples

- **Case Study 4-A**

Figure 3.15(a) shows the example which is 3-dimensional version of Fig. 3.4. In this case, the external load should be transmitted to one of 21 candidate loading locations along the external load direction. The structural domain is composed of 40×40×40 elements. The material properties and optimization parameters are same as those in Case Study 1 in Fig.

3.4. Figure 3.15(b) shows the best solution among all possible optimal layouts for loads applied at all possible candidate locations. The iteration histories and intermediate layouts during optimization iterations are shown Fig. 3.16(a). The values of the constraint functions shown in Fig. 3.16(b) converge to the target values stably.

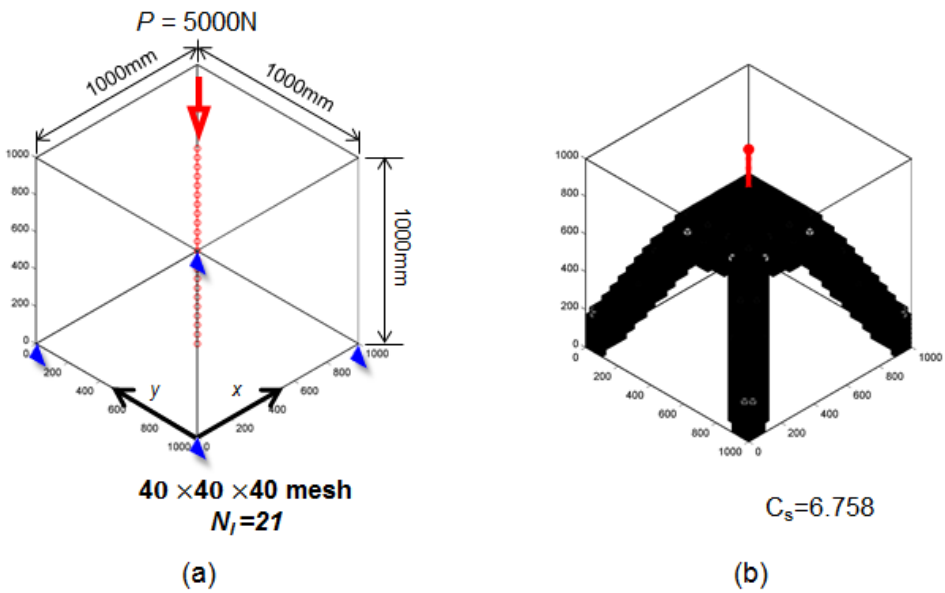

Fig. 3.15 Case study 4-A for a 3-dimensional version of case study 1 in Fig. 3.4: (a) Design domain with prescribed load/boundary conditions, and (b) the result by the proposed simultaneous optimization method.

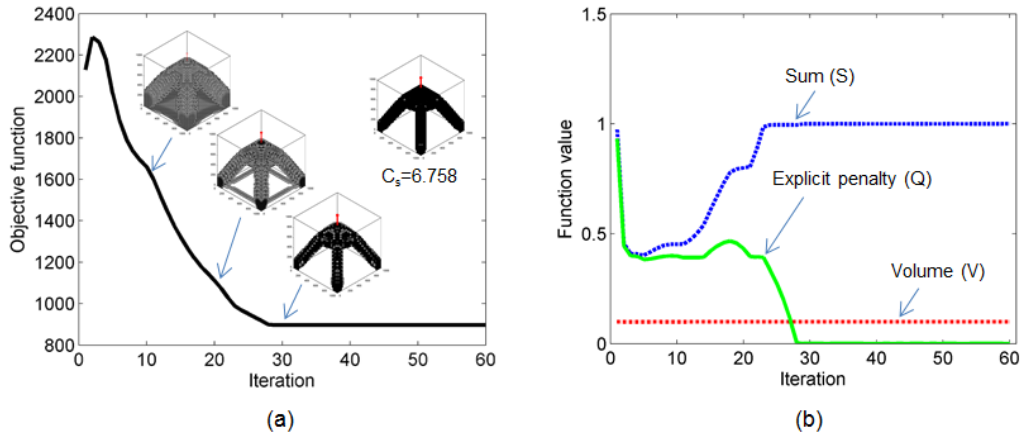

Fig. 3.16 Iteration history for Case study 4-A: (a) The objective function, and (b) the constraint functions.

- **Case Study 4-B**

Figure 3.17(a) shows the example which is 3-dimensional version of Fig. 3.6. In this case, the external load is transmitted to one of 16 candidate loading locations on the perpendicular plane to external load. The structural domain is composed of 32×32×64 elements. The material properties and parameters in optimization setup are the same as those in case study 2-A in Fig. 3.6, but $\overline{V}^* = 20$ %. Figure 3.17(b) shows the optimal solution by the developed simultaneous optimization method. In this problem, the optimal loading location and the structural topology are similar to that in case study 2-A shown in Fig. 3.6(c). The iteration histories and intermediate layouts during optimization iterations are shown Fig. 3.18(a) and the constraint functions in Fig. 3.18(b) converge to the target values stably.

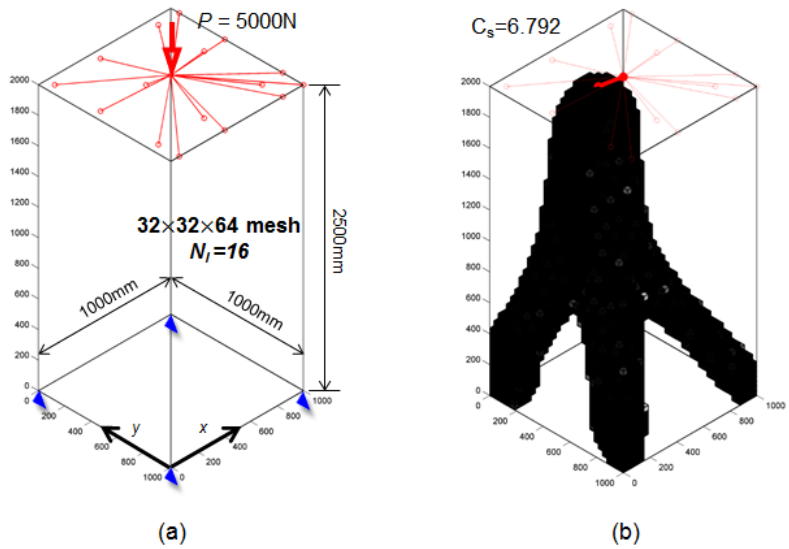

Fig. 3.17 Case study 4-B for a 3-dimensional version of case study 2-A in Fig. 3.6: (a) Design domain with prescribed load/boundary conditions, and (b) the result by the proposed simultaneous optimization method.

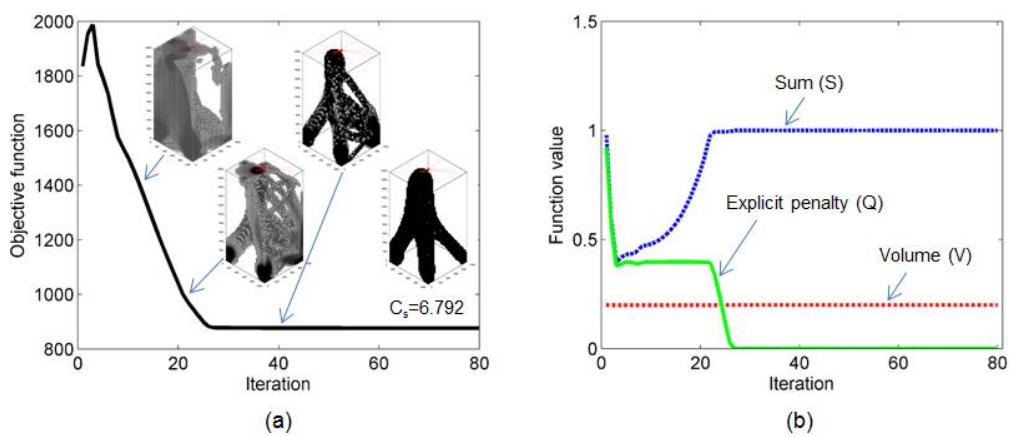

Fig. 3.18 Iteration history for case study 4-B: (a) The objective function, and (b) the constraint functions.

3.5 More discussions on the determination of the optimal loading location

So far, the developed simultaneous optimization method of the loading location and structural topology is based on the single loading point determination. It is because we focus on the concern to the practical engineering problem such as the determination of the optimal actuator location in the construction equipment frame. However, if upper bound of the constraint function, $S(\boldsymbol{\mu})$ in Eq. (3.11), is modified or we define the problem as the symmetric load condition, design of multiple loading location can be possible. Case studies for the multiple loading point design are described in Appendix. B. These kinds of problems are, for example, as bellows:

- One applied load is connected to two optimized locations under symmetric load condition. In this case, load design variable μ_i is converged to the values of 0.5 and 0.5.
- Two applied load is converged to two load location. In this case, the upper bound of Eq. (3.11) should be modified to the value of 2. But, meaningful solution can be obtained only under special design condition.

The effectiveness and usefulness is demonstrated and validated through various types of case studies. Extension to the multiple load case and three-dimensional structural domain problem can be treated without any difficulties. Modeling technique using the spring elements for the load connectivity has the great advantage in dealing with large size of engineering design practices because the implementation with the commercial finite element software is rather straightforward.

Although there are some inefficiency in form of the global stiffness equation using the Lagrange multiplier in Eq. (3.8) because it does not guarantee it positive definite, this is not the critical issue when the proposed method is implemented with the efficient commercial finite element analysis solver.

There are two tuning parameters in the proposed method. Careful selection of the parameters should be made, but their ranges are relatively small and typical ranges are suggested in Appendix. A.1. It is more efficient to do parameter study using the proposed method than to run the standard topology optimization for all the candidate loading locations.

The developed simultaneous optimization method is the gradient-based optimization, therefore, global optimal solution is not guaranteed. Global search algorithm such as the genetic algorithm can be adapted as a hybrid formulation. For example, loading point determination is optimized by the genetic algorithm and structural topology optimization is performed by the gradient method. Hybrid formulation is expected to be more effective when the candidate loading points become extremely large..

Chapter 4.

Integrated topology optimization considering actuator layout and weld manufacturability

4.1 Chapter overview

In this chapter, topology optimization technique for the simultaneous design of actuator layout and structure is integrated with weld manufacturability. There are two major issues in the application of the topology optimization framework to the frame structure of construction equipment. The first one was addressed in the previous chapter. As mentioned earlier, topology optimization with weld manufacturability in an early design stage is not the case of welding line reduction and welded joint specification; this is the problem of interpreting optimization results so effectively as to adapt them to the detailed design. In this point of view, manufacturing requirement such as avoiding typical truss structure should be investigated.

Among the previous works related to the manufacturing constraints of topology optimization, a method to extract optimal plate-like structures from a solid mesh [33] is most relevant to the weld manufacturability issue. Although the main idea comes from those of casting manufacturing constraint [32, 34], it generates similar material layout effectively similar to the welded structures consisting of several plates. In this study, a method of dividing the whole design domain into several subdomains and then projecting

the element design variables on the nodes of pre-defined plane is suggested.

To deal with sufficiently large size of problem for actual engineering practices, an interface between commercial CAE software (such as *ABAQUS*) and optimization code (developed in this investigation by *MATLAB*) is necessary. Thereby, the topology optimization framework using the ABAQUS-MATLAB interface is developed and verified throughout this chapter. Integrated with the simultaneous optimization of a loading point and structural topology, a topology optimization method providing plate-like structures is implemented. Several numerical examples are treated to show the validness of the developed code, such as compliance minimization problems and a problem of simplified version of a wheel loader frame with a modal frequency constraint.

The procedure of topology optimization for welded structures using the *ABAQUS-MATLAB* interface is shown in the next section. The integration with the simultaneous optimization technique of a loading point determination and structural topological layouts is followed in the following. The proposed integrated topology optimization method is verified through several design examples.

4.2 Topology optimization for welded structure

4.2.1 Plate-like topology optimization

The standard topology optimization problem is stated as:

$$\begin{aligned} &\underset{\boldsymbol{\rho}\in\mathbf{R}^n}{\text{Min.}}\ \mathbf{F}^T\mathbf{u} \\ &\text{s. t.}\ \ \sum_{e\in\Omega}\rho^e v^e \le V^* \\ &\qquad \mathbf{F}=\mathbf{K}(\boldsymbol{\rho})\mathbf{u} \\ &\qquad \rho_{\min}\le\rho^e\le\rho_{\max} \end{aligned}, \tag{4.1}$$

where, $\mathbf{F}$ is the applied load vector, $\mathbf{K}$ is the global stiffness matrix and $\mathbf{u}$ is the global displacement vector. The volume of element e is denoted by v^e and ρ_{min}, ρ_{max} is the minimum and maximum allowable element density. Typically, the results of topology optimization in Eq. (4.1) are usually truss-like structure, as can be seen in the previous chapter. To avoid the formation of interior cavities, an extraction method to parameterize the design domain as to produce plate-like shapes can be formulated. Figure 4.1 illustrates a schematic diagram of the proposed plate-like shape extraction method. The design domain Ω is divided into subdomains $\Omega_i\ (i=1,...,N_d)$ as shown in Fig. 4.1(a), and pre-determined extraction directions n_i and projected planes S_i are set up for the design variable parameterization in Ω_i. The element design variables ρ^e in Ω_i are so projected into S_i as to have the same value along the direction of n_i as depicted in Fig. 4.1(b). Therefore, same design variables ρ^e along the extraction direction in each subdomain can be ensured. Fig. 4.1(c) illustrates typical plate-like conceptual image of the topological layout in the form of plate-like structural layouts under a bending load.

Independency of the size and shape of mesh in topology optimization is achieved by filtering techniques [42-44]. In this study, the density filter with physical length scale and linear projection function [43] is employed. The concept of density filter is schematically shown in Fig. 4.2.

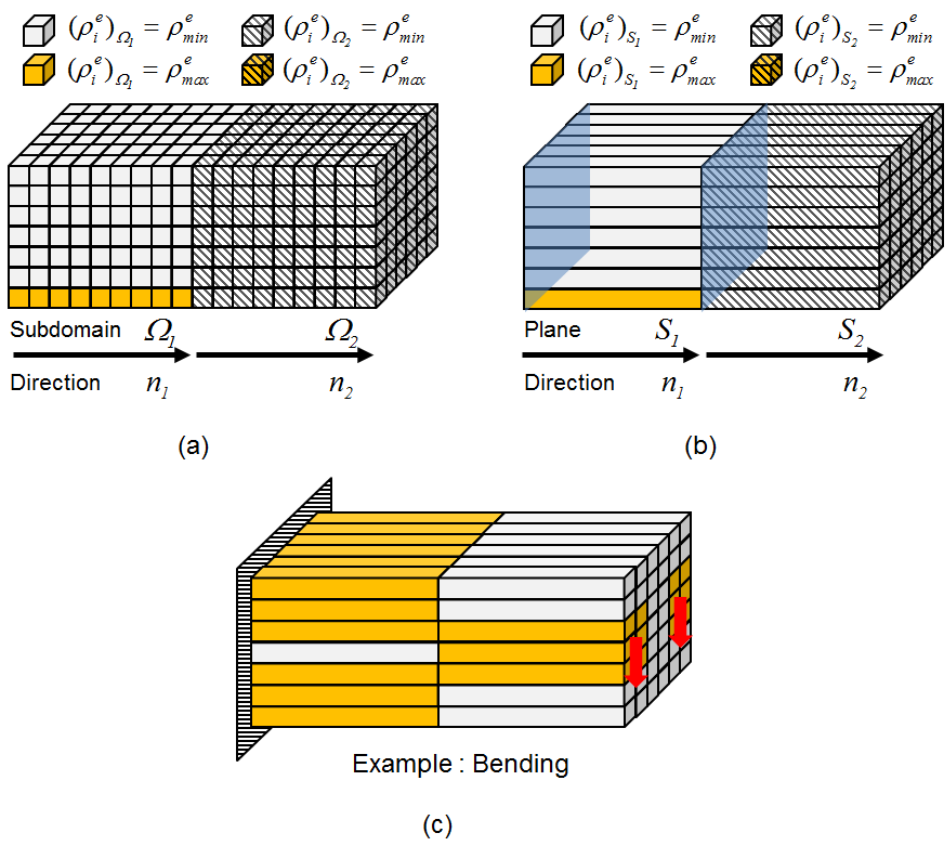

Fig. 4.1 Illustration of extracting plate-like structure in topology optimization by (a) dividing the entire domain into subdomains and setting extracting direction in each subdomain, and (b) projecting element design variables on the pre-defined plane and extracting it along the given direction. Typical plate-like shape of topological layout is (c).

Nodal densities ρ_j are the design variables in this method with the density filter; they should be converted into element densities ρ^e to enforce physical meaning. In a conversion process, the projection scheme, not influenced by mesh size, is based on a physical length scale $r_{\min}$. The projection functions should be constructed so that this parameter is equivalent to the minimum allowable radius. In Fig. 4.2(a), a circle of effective radius $r_{\min}$ centered at the centroid of element e is visualized to indicate the circular subdomain Ω_r^e contributed to the computation of ρ^e. A linear projection function performing a weighted average of the eligible nodal design variables determines a magnitude of 1 at the element centroid and decreases linearly to 0 over $r_{\min}$ as shown in Fig 4.2(b). This weight functions is defined by

$$w(\mathbf{x}-\overline{\mathbf{x}}^e)=\begin{cases}\dfrac{r_{\min}-r}{r_{\min}}, & \text{if } x\in\Omega_r^e\\ 0, & \text{otherwise}\end{cases}, \tag{4.2a}$$

$$r\equiv\left\|\mathbf{x}-\overline{\mathbf{x}}^e\right\|\le r_{\min}\quad, \tag{4.2b}$$

where, $\overline{\mathbf{x}}^e$ stands for the centroid of the element e. The element density ρ^e in Fig. 4 can be defined by

$$\rho^e=\frac{\sum_{j\in\Omega_r^e}\rho_j w(\mathbf{x}_j-\overline{\mathbf{x}}^e)}{\sum_{j\in\Omega_r^e}w(\mathbf{x}_j-\overline{\mathbf{x}}^e)} \tag{4.3}$$

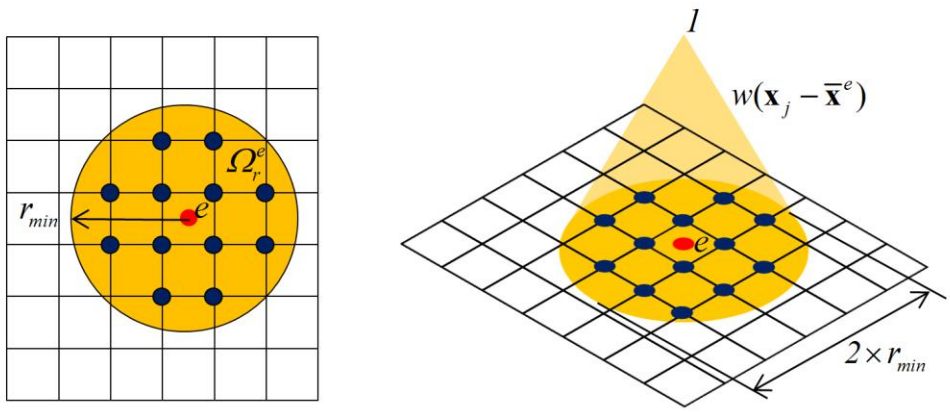

Fig. 4.2 Schematic concept of the density filter: (a) nodes inside the domain are used in the projection scheme, and (b) the weight function for the linear projection.

Incorporating with the density filter, the problem of topology optimization in Eq. (4.1) now can be expressed as a function of the nodal design variables $(\boldsymbol{\rho}_n)_s$ to enforce the results of topology optimization in the form of plate-like shape.

$$\begin{aligned} &\underset{(\boldsymbol{\rho}_n)_s \in \mathbf{R}^n}{\text{Min.}} \ \mathbf{F}^T\mathbf{u} \\ &\text{s.t.} \ \sum_{e\in\Omega} \rho^e((\boldsymbol{\rho}_\mathbf{n})_s)v^e \le V^* \\ &\mathbf{F} = \mathbf{K}((\boldsymbol{\rho}_\mathbf{n})_s)\mathbf{u} \\ &(\rho_n)_{min} \le (\rho_n)_s \le (\rho_n)_{max} \end{aligned} \quad , \tag{4.4}$$

4.2.2 Topology optimization using Matlab-Abaqus interface

The plate-like topology optimization code is implemented using the interface between *Matlab* and *Abaqus*. The procedure to carry out the topology optimization is summarized in Fig. 4.3. Notice that this in-house code is utilized for the integration of the optimization method developed in chapter 3 (*simultaneous optimization of a loading point and structural topology*) and the plate-like topology optimization method for the welded structure. Practical applications such as the design problem of construction equipment frame require efficient commercial FE solver for the large scale problem up to millions of degree of freedom. *Abaqus* is one of widely used commercial finite element solver.

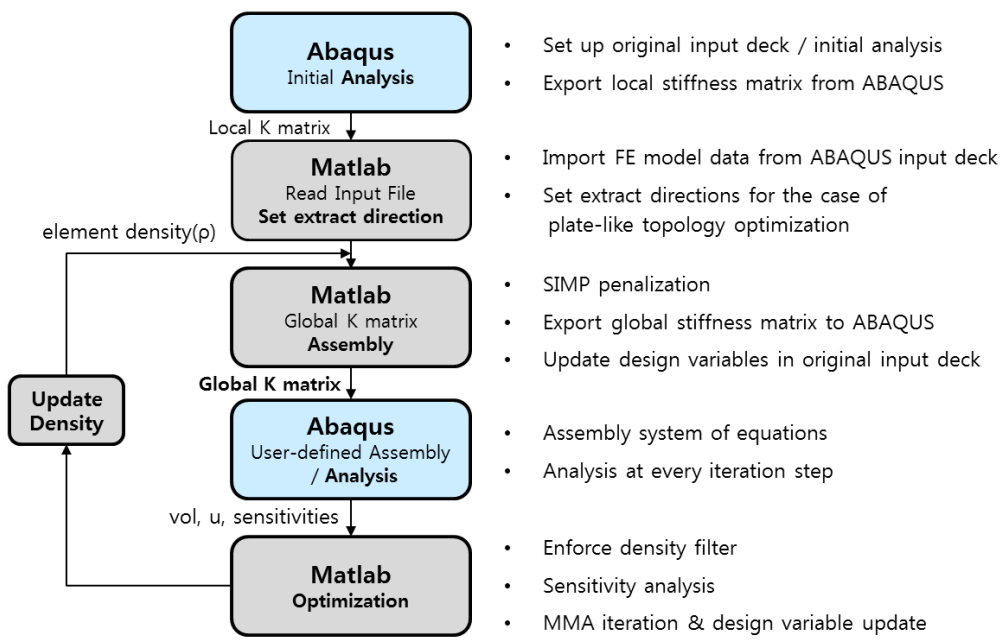

Fig. 4.3 Topology optimization procedure using *Matlab* - *Abaqus* interface

The interface is accomplished by the use of *Python* scripts for *Abaqus* [45]. The results of the topology optimization, the element-wise density design variable, are provided as the format of an *Abaqus* ODB output database file. This file can be read more conveniently by the commercial FE post processing software such as *Altair HyperView* because the treatment of the user-defined density variable is more straightforward.

Two types of optimization problems are examined in this section. One is compliance minimization problem with volume constraint and the other is, with constraints of volume and 1st eigenfrequency. Formulations for the former are in Eq. (4.1) for the case of standard topology optimization and in Eq. (4.4) for the case of plate-like topology optimization, respectively. The latter formulation for the standard topology optimization with 1st eigenfrequency constraint is expressed as

$$\begin{aligned} &\underset{\boldsymbol{\rho}\in\mathbf{R}^n}{\text{Min.}}\ \mathbf{F}^T\mathbf{u} \\ &\text{s.t.}\ \ \sum_{e\in\Omega}\rho^e v^e \le V^* \\ &\qquad (\omega_1)^2 \ge (\omega_1^*)^2 \\ &\qquad \mathbf{F}=\mathbf{K}(\boldsymbol{\rho})\mathbf{u} \\ &\qquad \mathbf{K}\phi_i=\omega_i^2\mathbf{M}\phi_i, \quad i=1,\ldots N \\ &\qquad \rho_{\min}\le\rho^e\le\rho_{\max} \end{aligned} \quad , \tag{4.5}$$

where, ω_i^2 is the i-th eigenvalue and ϕ_i the corresponding eigenvector, and $\mathbf{M}$ is the global mass matrix. Eigenfrequency f_i can be calculated from the relation $\omega_i = 2\pi f_i$. Likewise, the plate-like topology optimization problem minimizing structural compliance with volume and modal frequency constraint can be formulated as Eq. (4.6).

$$
\begin{aligned}
&\underset{(\boldsymbol{\rho}_n)_s \in \mathbf{R}^n}{\text{Min.}} \ \mathbf{F}^T\mathbf{u} \\
&\text{s.t.} \ \sum_{e\in\Omega} \rho^e((\boldsymbol{\rho}_\mathbf{n})_s)v^e \le V^* \\
&\quad (\omega_1(\boldsymbol{\rho}_\mathbf{n})_s)^2 \ge (\omega_1^*(\boldsymbol{\rho}_\mathbf{n})_s)^2 \qquad , \\
&\quad \mathbf{F} = \mathbf{K}((\boldsymbol{\rho}_\mathbf{n})_s)\mathbf{u} \\
&\quad \mathbf{K}((\boldsymbol{\rho}_\mathbf{n})_s)\phi_i = \omega_i^2\mathbf{M}((\boldsymbol{\rho}_\mathbf{n})_s)\phi_i, \quad i = 1,...N \\
&\quad (\rho_n)_{\min} \le (\rho_n)_s \le (\rho_n)_{\max}
\end{aligned}
\tag{4.6}
$$

The gradient-based optimizer MMA [41] is used throughout this work. Sensitivity analysis should be made to update the design variable. Sensitivities of structural compliance $C = \mathbf{F}^T\mathbf{u}$, objective function in Eq. (4.1) is well-known [4, 24, 40, 43] in the following form as

$$
\frac{\partial C}{\partial \boldsymbol{\rho}} = -\mathbf{u}^T \frac{\partial \mathbf{K}(\boldsymbol{\rho})}{\partial \boldsymbol{\rho}}\mathbf{u} \, . \tag{4.7}
$$

In the equation (4.7), the global stiffness matrix $\mathbf{K}$ with the SIMP penalization is expressed by

$$
\mathbf{K} = \sum_{i=1}^{N_e} \rho_i^p \mathbf{k}_i^0 \, , \tag{4.8}
$$

where p is the SIMP penalty parameter, $\mathbf{k}_i^0$ denotes the i-th element stiffness matrix, and N_e is total number of finite elements in the design domain. The sensitivity expression of compliance in nodal design variables in Eq. (4.7) is calculated using Eqs. (4.3), (4.7) and (4.8) as

$$
\frac{\partial C}{\partial (\boldsymbol{\rho}_\mathbf{n})_s} = -\mathbf{u}^T \frac{\partial \mathbf{K}((\boldsymbol{\rho}_\mathbf{n})_s)}{\partial (\boldsymbol{\rho}_\mathbf{n})_s}\mathbf{u}\frac{\partial \rho^e}{\partial (\boldsymbol{\rho}_\mathbf{n})_s} = -p\boldsymbol{\rho}_\mathbf{n}^{(p-1)}\mathbf{u}^T \frac{\partial \mathbf{K}((\boldsymbol{\rho}_\mathbf{n})_s)}{\partial (\boldsymbol{\rho}_\mathbf{n})_s}\mathbf{u}\frac{\partial \rho^e}{\partial (\boldsymbol{\rho}_\mathbf{n})_s} \, . \tag{4.9}
$$

Before dealing with the sensitivity expression in modal frequency problems, it is worthwhile to discuss the issue, which is one of main problem in the topology optimization of modal frequencies; possibility of localized modes in low density areas [7, 13, 46]. Localized mode can occur in areas that are near minimum densities during the optimization process because they are very flexible compared to elements with full densities. This localized mode should be prevented by specialized SIMP penalization scheme; otherwise they control the lowest eigenmode of the whole structure. In the study, material interpolation scheme suggest by Du and Olhoff [7] is applied to remove them. The global mass matrix $\mathbf{M}$ of the finite element with the SIMP penalization can be expressed in the same manner with Eq. (4.8) as

$$\mathbf{M} = \sum_{i=1}^{N_e} \mathbf{m}_i(\rho_i) = \sum_{i=1}^{N_e} \rho_i^q \mathbf{m}_i^0 , \tag{4.10}$$

where $\mathbf{m}_i$ represents the i-th element mass matrix, $\mathbf{m}_i^0$ denote the i-th element mass matrix corresponding to fully solid material, and q is the SIMP penalty parameter for the mass matrix. To eliminate the localized eigenmodes, Eq. (4.10) is replaced by Eq. (4.11) in order to set the element mass very low value via a higher penalization parameter in subregions with low local density and ensure C^1 continuity of the interpolation model as

$$\mathbf{m}_i(\rho_i) = \begin{cases} \rho_i \mathbf{m}_i^0, & \rho_i > 0.1 \\ (c_1\rho_i^6 + c_2\rho_i^7)\mathbf{m}_i^0, & \rho_i \le 0.1 \end{cases}, \tag{4.11}$$

where the coefficients are $c_1 = 6\times10^5$ and $c_2 = -5\times10^6$.

The sensitivity of eigenvalue ω_i^2 for the standard topology optimization [7, 13, 40] can be obtained by

$$\frac{\partial \omega_i^2}{\partial \boldsymbol{\rho}} = \boldsymbol{\phi}_i^T \left(\frac{\partial \mathbf{K}(\boldsymbol{\rho})}{\partial \boldsymbol{\rho}} - \omega_i^2 \frac{\partial \mathbf{M}(\boldsymbol{\rho})}{\partial \boldsymbol{\rho}} \right) \boldsymbol{\phi}_i \ . \tag{4.12}$$

Likewise, the sensitivity equation of plate-like topology optimization is expressed by

$$\frac{\partial \omega_i^2}{\partial (\boldsymbol{\rho}_\mathbf{n})_s} = \boldsymbol{\phi}_i^T \left(\frac{\partial \mathbf{K}((\boldsymbol{\rho}_\mathbf{n})_s)}{\partial (\boldsymbol{\rho}_\mathbf{n})_s} - \omega_i^2 \frac{\partial \mathbf{M}((\boldsymbol{\rho}_\mathbf{n})_s)}{\partial (\boldsymbol{\rho}_\mathbf{n})_s} \right) \boldsymbol{\phi}_i \ \frac{\partial \rho^e}{\partial (\boldsymbol{\rho}_\mathbf{n})_s} \ . \tag{4.13}$$

In equations (4.12) and (4.13), the derivatives of the matrices $\mathbf{K}$ and $\mathbf{M}$ can be calculated explicitly from the SIMP penalization model in Eqs. (4.8) and (4.11). Therefore, the sensitivity expression of Eqs. (4.12) and (4.13) becomes

$$\frac{\partial \omega_i^2}{\partial \boldsymbol{\rho}} = \boldsymbol{\phi}_i^T \left(p\boldsymbol{\rho}^{(p-1)} \frac{\partial \mathbf{K}(\boldsymbol{\rho})}{\partial \boldsymbol{\rho}} - \omega_i^2 q\boldsymbol{\rho}^{(q-1)} \frac{\partial \mathbf{M}(\boldsymbol{\rho})}{\partial \boldsymbol{\rho}} \right) \boldsymbol{\phi}_i \ , \tag{4.14a}$$

$$\frac{\partial \omega_i^2}{\partial (\boldsymbol{\rho}_\mathbf{n})_s} = \boldsymbol{\phi}_i^T \left(p(\boldsymbol{\rho}_\mathbf{n})_s^{(p-1)} \frac{\partial \mathbf{K}((\boldsymbol{\rho}_\mathbf{n})_s)}{\partial (\boldsymbol{\rho}_\mathbf{n})_s} - \omega_i^2 q(\boldsymbol{\rho}_\mathbf{n})_s^{(q-1)} \frac{\partial \mathbf{M}((\boldsymbol{\rho}_\mathbf{n})_s)}{\partial (\boldsymbol{\rho}_\mathbf{n})_s} \right) \boldsymbol{\phi}_i \ \frac{\partial \rho^e}{\partial (\boldsymbol{\rho}_\mathbf{n})_s} \ . \tag{4.14b}$$

4.2.3 Numerical examples

In this section, numerical examples will be considered to verify the validness and effectiveness of the proposed method. Three case studies having different geometry and load condition are presented. In case 1, compliance minimization for L-type beam is examined. Comparison is made between the results of the commercial optimization software, *Altair OptiStruct*, and those of the developed in-house code with *Matlab-Abaqus* interface. Case 2 is a kind of a feasibility test whether the proposed method can

be applied to the frame structures or not. Compliance minimization for a simple ladder type frame structure is investigated. In case 3, simplified example of a wheel loader frame design will be demonstrated to show the possibility of application to the actual engineering practice. Compliance minimization problem with constraints of volume and 1st modal frequency is formulated, as described in Eqs. (4.5) and (4.6). As mentioned earlier, the density filtering technique with the minimum allowable radius $r_{\min}$ is applied. Note that the values of $\rho_{\max} = (\rho_n)_{\max} = 1$, $\rho_{\min} = (\rho_n)_{\min} = 0.001$ and $p = 3$ for the penalty parameters are used throughout this section.

- **Case Study 1**

The design domain given in Fig. 4.3 is divided into 3 sub domains for the plate-like topology optimization. One of 3 sub domains is a sub domain utilized for the connection area between Ω_1 and Ω_2, thus remains as the region where the standard topology optimization scheme is applied. On the other hand, in case of the standard topology optimization as formulated in Eq. (4.1), the whole domain is used as the design domain. Information of the finite element analysis is in the following.

- **Finite element model information**

Element type in Abaqus: C3D8 [45]

Element type in OptiStruct: CHEXA [36]

Number of Elements: 72,000

Number of Nodes: 79,821

Young's Modulus: 2.1×10^5

Poisson's ratio: 0.30

Density ρ_0: 7.9×10^{-9}

Topology optimization parameters are summarized below. The optimized problem for case study 1 is formulated as Eq. (4.1) in the standard topology optimization case and Eq. (4.4) in the plate-like topology optimization case.

- **Optimization information**

Upper bound of volume constraint V^*: $0.10 \times V^0$

Filter radius $r_{\min}$: 7.5 (1.5 times of the average element size)

Figure 4.5 shows the distribution of the element density ($\rho^e \geq 0.2$) of the standard topology optimization results. The result by using *OptiStruct* is illustrated in Fig. 4.5(a) and one by the developed code with *Matlab-Abaqus* interface is depicted in Fig. 4.5(b). The element density contour of the result by the similar process using *OptiStruct* (with extrusion manufacturing constraint [36]) with the plate-like topology optimization is in Fig. 4.6(a). Figure 4.6(b) shows the result by the developed code. The density distribution agrees reasonably with each other. These results demonstrate the validity of the developed in-house code.

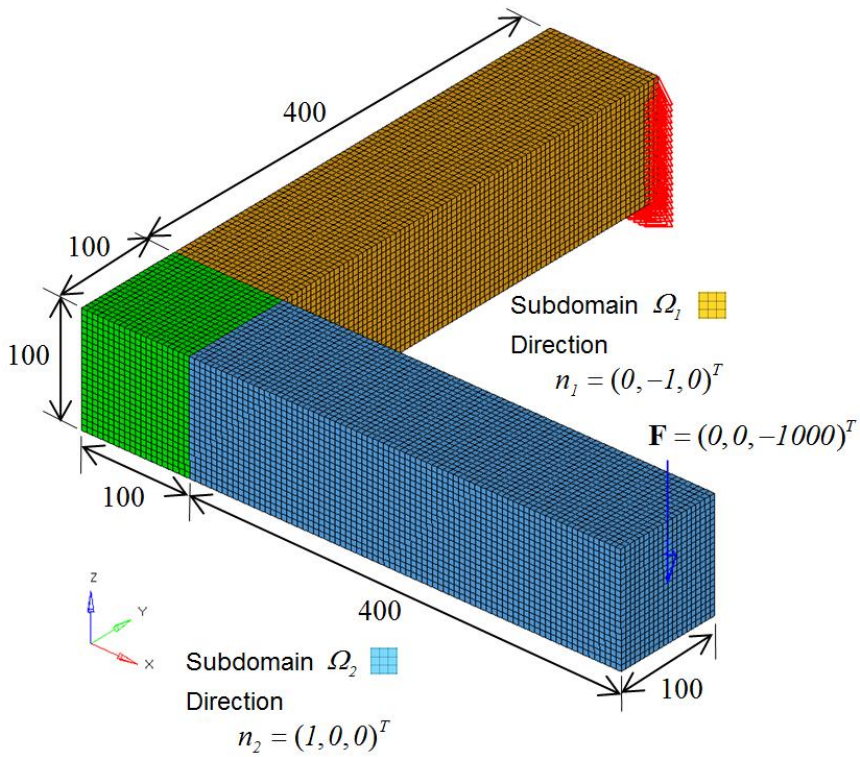

Fig. 4.4 Case study 1 for plate-like topology optimization in L-shape domain

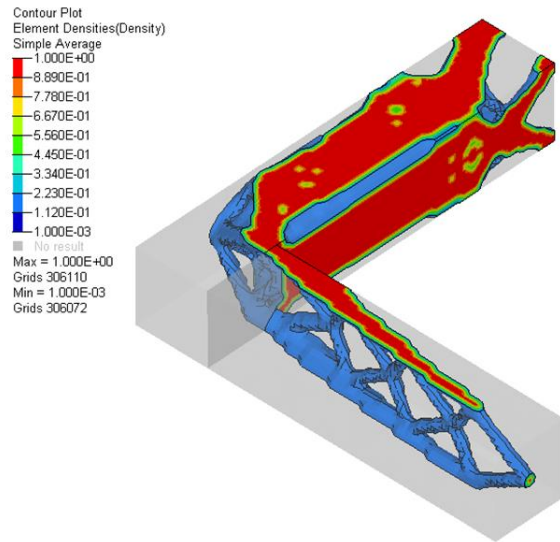

(a)

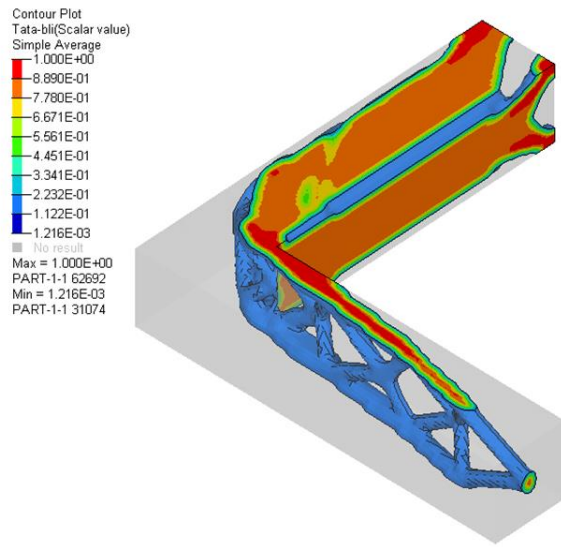

(b)

Fig. 4.5 Standard topology optimization results for case study 1 (a) by *OptiStruct*, and (b) by the developed code using *Matlab-Abaqus* interface.

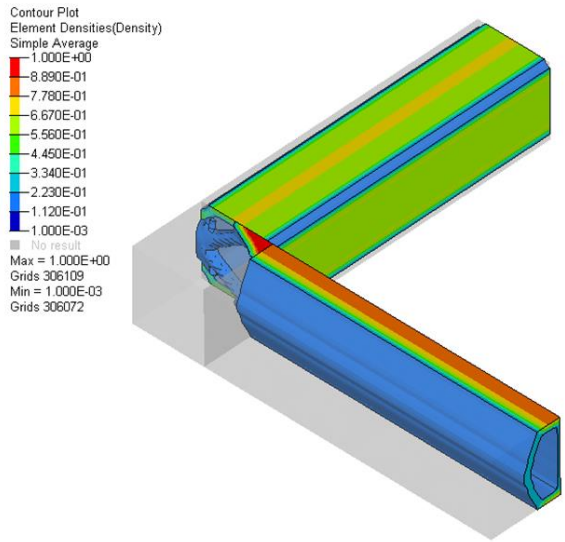

(a)

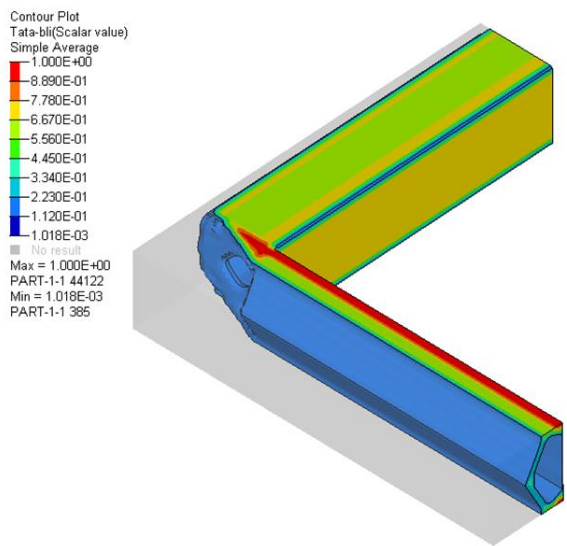

(b)

Fig. 4.6 Plate-like topology optimization results for case study 1 (a) by *OptiStruct*, and (b) by the developed code using *Matlab-Abaqus* interface.

- **Case Study 2**

The design domain given in Fig. 4.7 is divided into 13 sub domains for the case of plate-like topology optimization and extract directions are illustrated also. There are two directions of extraction, those of $\Omega_1 \sim \Omega_{10}$ are $x-$direction and the others $y-$direction. In case of the standard topology optimization, the whole domain is used as the design domain. Information of the finite element analysis and parameters on topology optimization is summarized in the following. The formulation is the same as Eqs. (4.1) and (4.4).

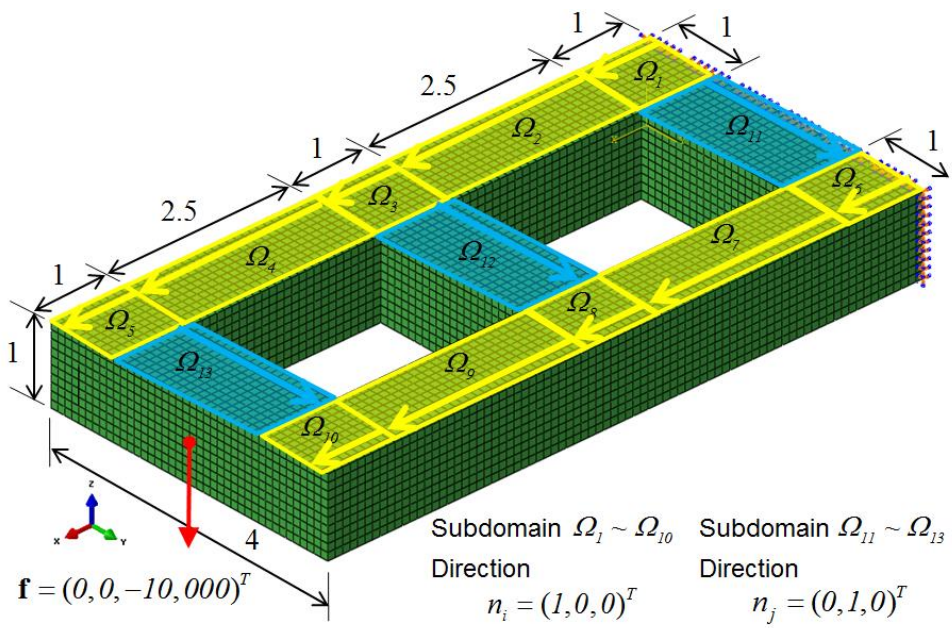

Fig. 4.7 Case study 2 for plate-like topology optimization in ladder-shape domain

- **Finite element model information**

Element type in Abaqus: C3D8

Number of Elements: 22,000

Number of Nodes: 26,499

Young's Modulus: 2.068×10^{11}

Poisson's ratio: 0.29

Density ρ_0: 7820

- **Optimization information**

Upper bound of volume constraint V^*: $0.15\times V^0$

Filter radius $r_{\min}$: 0.15 (1.5 times of the average element size)

Figure 4.8 shows the distribution of the element density ($\rho^e \geq 0.3$) of the topology optimization results. The result of the standard topology optimization case is illustrated in Fig. 4.8(a) and one by the plate-like topology optimization is depicted in Fig. 4.8(b). Definitely, the result in Fig. 4.8(b) can provide much better convenience to interpret to the detailed design process when the result is preferred to be manufactured by the welding process. In this example, cross members make little contribution to the bending stiffness, therefore they disappeared in both cases shown in Fig. 4.8(a) and 4.8(b).

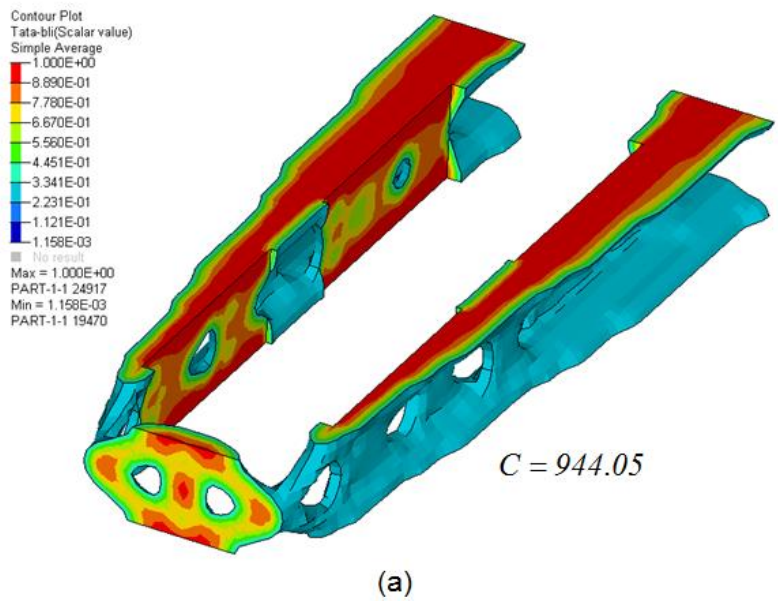

(a)

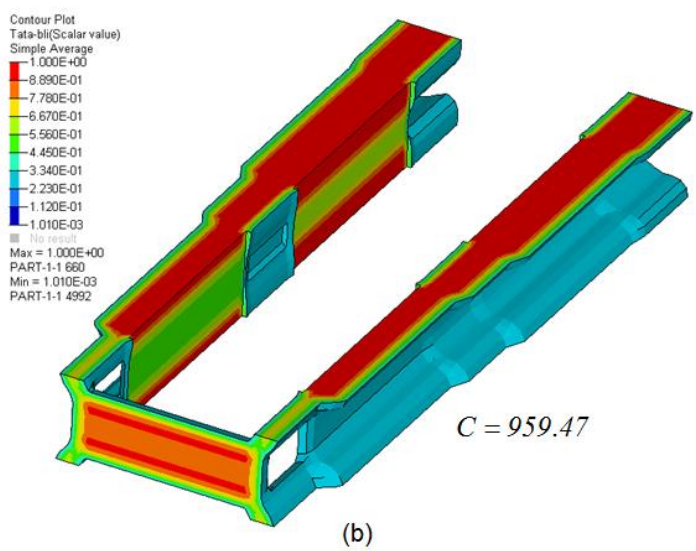

(b)

Fig. 4.8 The topology optimization results for case study 2 (a) by the standard method, and (b) by the plate-like method.

- **Case Study 3**

Figure 4.9 shows the example of simplified wheel loader frame structure. The design domain is divided into 7 sub domains for the plate-like topology optimization and corresponding extract directions are given in Fig. 4.9(a). Two load cases, one is shown in Fig. 4.9(a) and the other in Fig. 4.9(b), are defined in this example. Information of the finite element analysis and parameters on topology optimization is summarized in the following. The formulation is same as Eq. (4.5) and (4.6) for the standard topology optimization and plate-like one, respectively.

- **Finite element model information**

Element type in Abaqus: C3D8

Number of Elements: 11,480

Number of Nodes: 14,441

Young's Modulus: 2.06×10^5

Poisson's ration: 0.29

Density ρ_0: 7.8×10^{-9}

- **Optimization information**

Upper bound of volume constraint V^*: $0.25\times V^0$

Lower bound of 1st eigenvalue $(\omega_1^*)^2$: $2\times\pi\times(50\ Hz)$

Filter radius $r_{\min}$: 75 (1.5 times of the average element size)

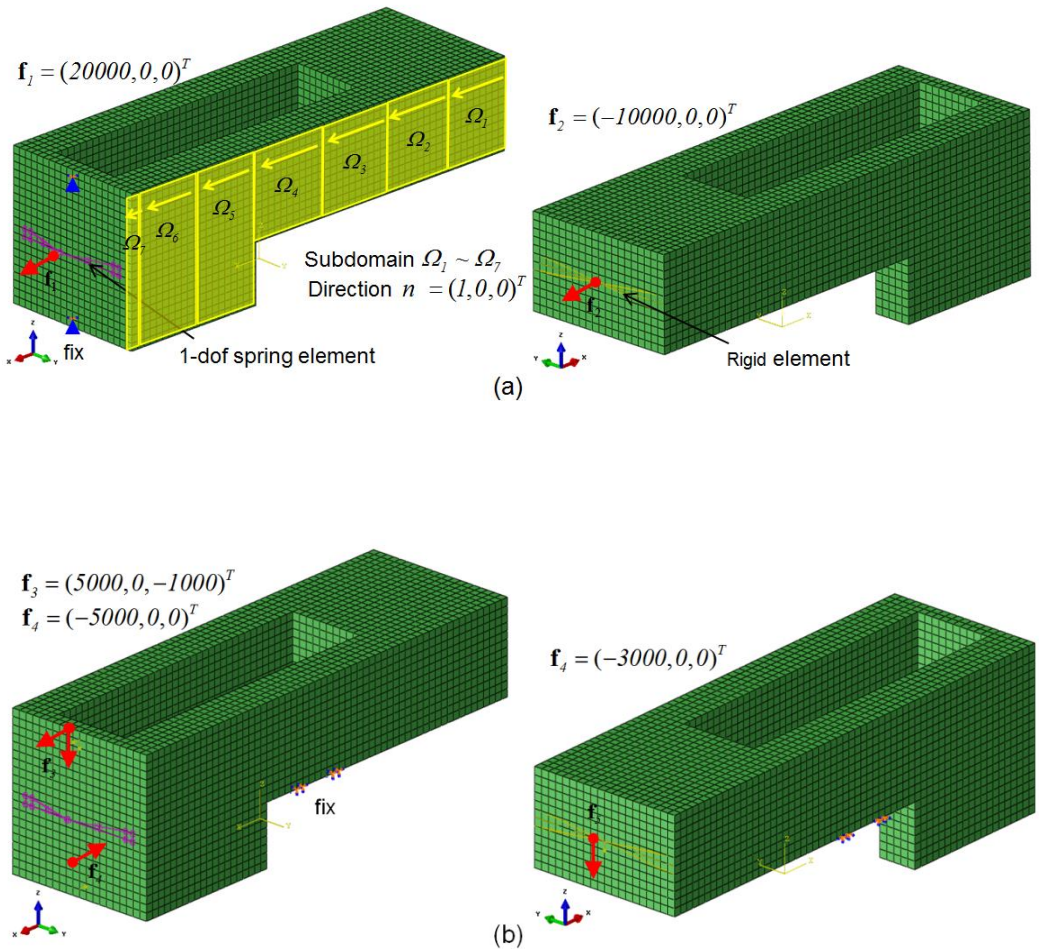

Fig. 4.9 Case study 3 for a simplified wheel loader frame domain: (a) load case 1 including illustration of sub domains for the plate-like topology optimization, and (b) load case 2

Figure 4.10 shows the distribution of the element density ($\rho^e \geq 0.3$) of the topology optimization results. The result of the standard topology optimization case is illustrated in Fig. 4.10(a) and one by the plate-like topology optimization is depicted in Fig. 4.10(b). Definitely, the result in Fig. 4.8(b) shows more possibility of interpretation to the welded structure design than that of the standard topology optimization. Although there is advantage in manufacturing point of view, the value of objective function (compliance) is a bit higher in the result of the plate-like topology optimization. Notice that there is a trade-off between the manufacturability and the structural performance. The constraint functions of volume and 1st eigenvalue become both active, which is, 1st modal frequency attained 50 Hz.

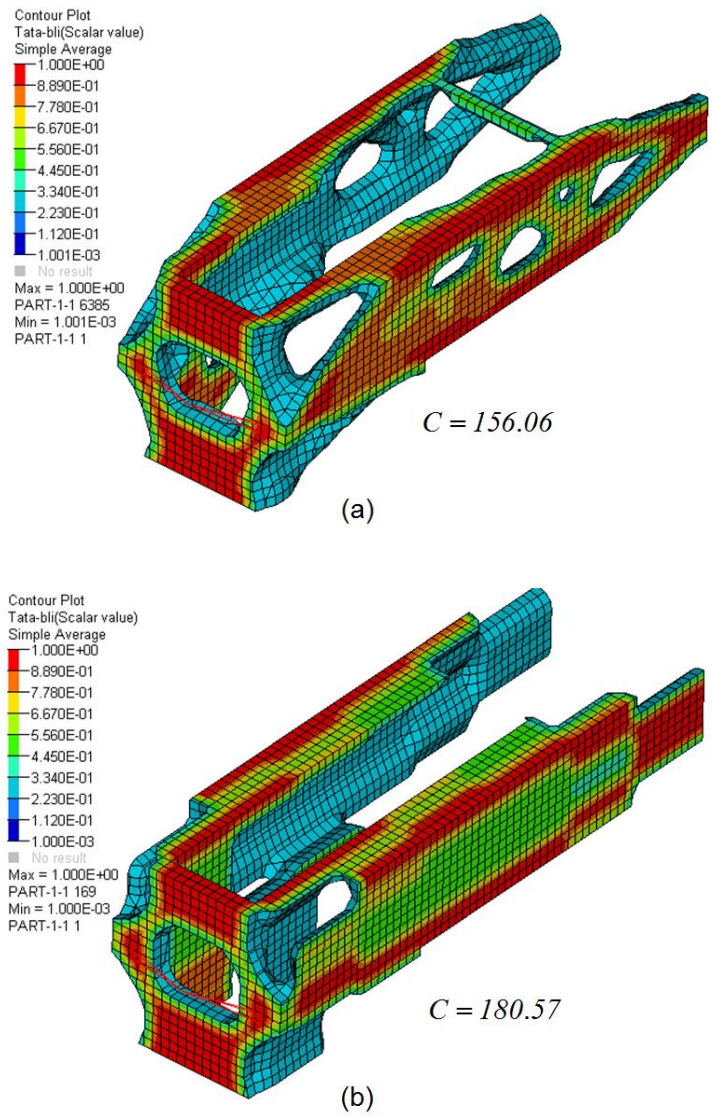

Fig. 4.10 Topology optimization results for case study 3 (a) by the standard method, and (b) by the plate-like method.

4.3 Integrated topology optimization for a frame structure

4.3.1 Implementation of simultaneous optimization of a loading location and structural topology

The topology optimization method developed in chapter 3, which is, the simultaneous optimization of a loading point and structural topology, is integrated with the plate-like topology optimization method described in section 4.2. Overall procedures are basically same as described in Fig. 4.3, but some care must be taken due to the special modeling technique and formulation of the simultaneous design optimization problem suggested in chapter 3.

The loading point connection is proposed to be modeled by 1-dof spring element in section 3.2., and the stiffness of the spring element is suggested to be lower than 10% of the maximum diagonal term of the continuum element stiffness. This relatively low spring stiffness makes the fundamental eigenvalues of the whole system very low compared to those of the continuum structure. In this situation, one cannot select the exact eignemode to be optimized. To overcome this difficulty, independent ABAQUS input deck for the modal analysis is prepared during the optimization. Spring elements are removed in independent modal input deck because the eigenmode in continuum structure alone is practically important in the optimization process. The spring elements are required only for the load connectivity in the static analysis. Due to this additional modal input deck, total analysis cost may increase but, we do not suffer from considering the coupling eigenmode between continuum structure and spring elements for the load

connectivity. This modified procedure is summarized in Fig. 4.11.

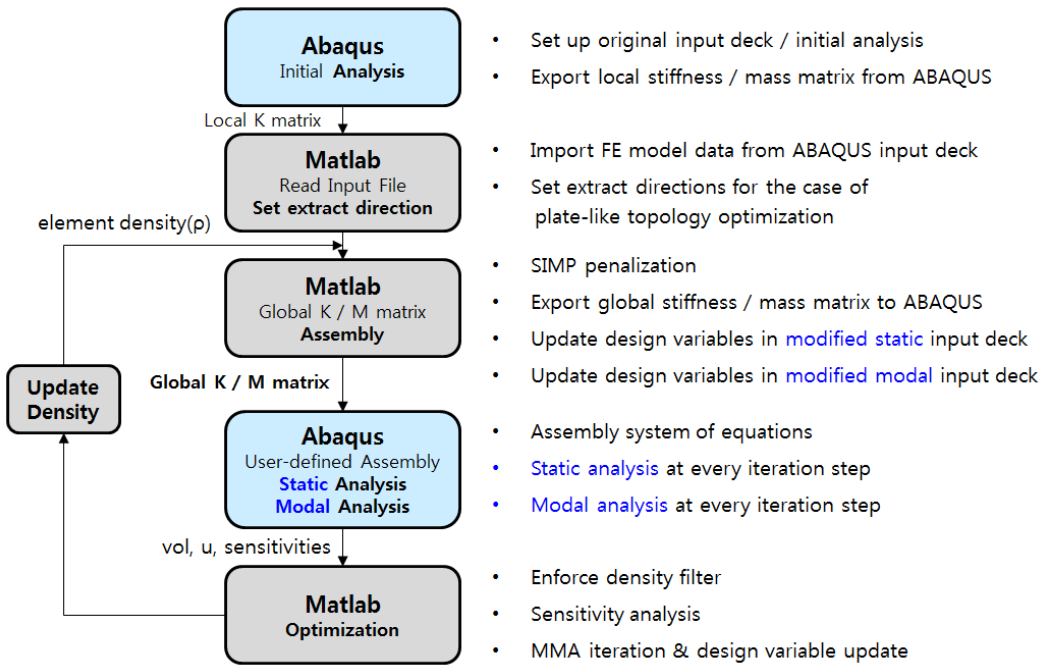

Fig. 4.11 Modified procedure for the integrated topology optimization

Thus, proposed integrated topology optimization is formulated as

$$\underset{\boldsymbol{\mu}\in\mathbf{R}^{N_l},(\boldsymbol{\rho}_n)_s\in\mathbf{R}^{N_e}}{\text{Minimize}} \quad \ln\left[\left\{C_l(\boldsymbol{\mu},(\boldsymbol{\rho}_n)_s)+1\right\}\left\{C_s(\boldsymbol{\mu},(\boldsymbol{\rho}_n)_s)+1\right\}\right], \tag{4.15}$$

$$\begin{aligned} \text{subject to} \quad & V(\boldsymbol{\rho}) = \sum_{j=1}^{N_e} \rho_j((\boldsymbol{\rho}_\mathbf{n})_s)V_j / V_s^* \le 1 \\ & (\omega_i(\boldsymbol{\rho}_\mathbf{n})_s)^2 \ge (\omega_i^*(\boldsymbol{\rho}_\mathbf{n})_s)^2 \\ & S(\boldsymbol{\mu}) = \sum_{i=1}^{N_l} \mu_i \le 1 \\ & Q(\boldsymbol{\mu}) = \sum_{i=1}^{N_l} \mu_i(1-\mu_i) \le \delta \end{aligned} \quad . \tag{4.16}$$

For simplicity, governing equation and side constraints were omitted in Eqs. (4.15) and (4.16).

4.3.2 Numerical examples

Two case studies for validation of the integrated topology optimization are considered. The first is the similar one as in Fig. 3.17, the other is for the simplified wheel loader frame example which is treated in Fig. 4.9. From these examples, one can find the usefulness of the proposed integrated topology optimization. The values of $\rho_{\max} = (\rho_n)_{\max} = 1,\ \rho_{\min} = (\rho_n)_{\min} = 0.001$ and $\eta = p = 3$ for the penalty parameters are used throughout these examples.

- **Case Study 1**

The structural and load design domains are given in Fig. 4.12, which is the same domains discussed in Fig. 3.17 except the element discretization of the structural domain. The whole structural domain is divided into 5 sub domains for the plate-like topology optimization and the loading location can move to one of 16 candidate loading points on top surface. The extract directions of the plate-like topology optimization are all $z-$ direction. Information of the finite element analysis and parameters on topology optimization is summarized in the following.

- **Finite element model information**

Element type in Abaqus: C3D8

Number of Elements: 2,000

Number of Nodes: 2,542

Young's Modulus: 2.1×10^5

Poisson's ration: 0.3

Density ρ_0: 7.8×10^{-9}

Stiffness of the spring element k_0: 4×10^{5}

- **Optimization information**

Upper bound of volume constraint V^*: $0.25\times V^0$

Lower bound of 1st eigenvalue $(\omega_1^*)^2$: $2\times\pi\times(160\ Hz)$

Upper bound of explicit penalty function δ: 0.7

Filter radius $r_{\min}$: 15 (1.5 times of the average element size)

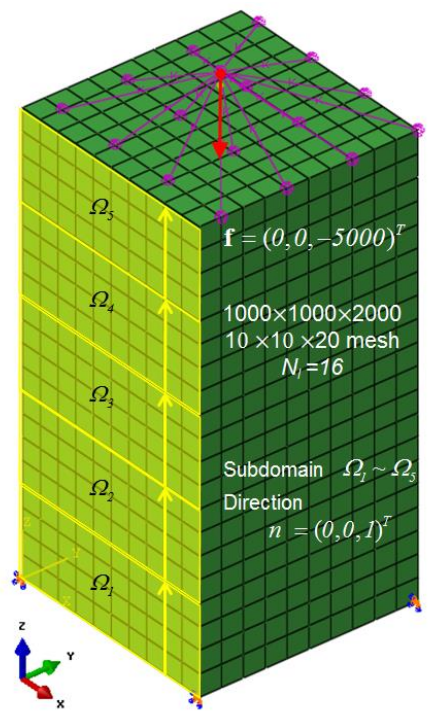

Fig. 4.12 Case study 1 for the integrated topology optimization; a horizontally-movable load case in Fig. 3.17

Figure 4.13 shows the distribution of the element density ($\rho^e \geq 0.3$) of the topology optimization results. The result of the standard topology optimization case is shown in Fig. 4.13 and one by the plate-like topology optimization is depicted in Fig. 4.14. The simultaneous optimization of a loading point determination and structural topology is clearly achieved in both results and the plate-like topology optimization can be seen in Fig 4.14. The result in Fig. 4.14 provides possibility of interpretation to the welded structure design than that of the standard topology optimization case in Fig. 4.15. Also, the value of objective (compliance) is a little higher in the result of the plate-like topology optimization due to the "plate-like" shape constraint.

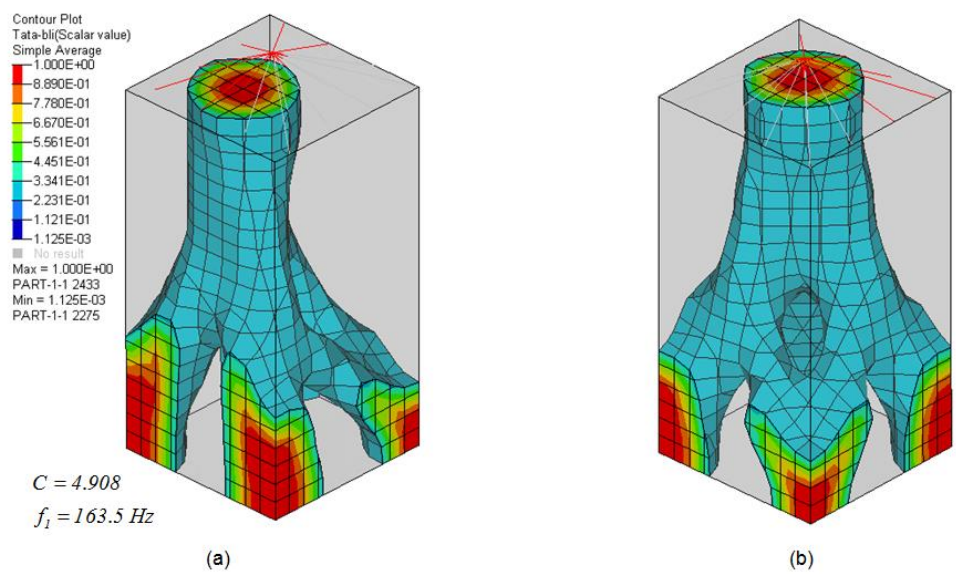

Fig. 4.13 Result of the integrated topology optimization for case study 1: standard case in (a) front iso view, and (b) rear iso view..

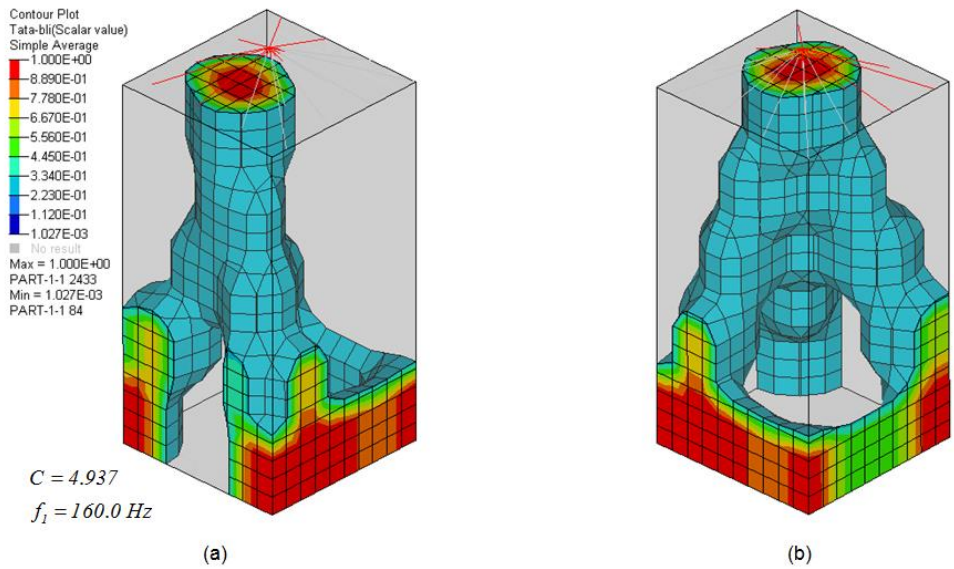

Fig. 4.14 Result of the integrated topology optimization for case study 1: standard case in (a) front iso view, and (b) rear iso view.

- **Case Study 2**

The problem description given in Fig. 4.15 is similar one discussed in Fig. 4.9. The structural design domain, loading condition and finite element modeling information are the same with the case in Fig. 4.9, except the external load $\mathbf{f}_1$, corresponding to cylinder force, is connected to 32 candidate loading locations. Because of the symmetry of cylinder load, two loading locations should be simultaneously determined with the structural topology. Thus, upper bounds of constraint functions in Eq. (4.16) are modified to two times of the case in Fig 4.9. Different numbers of sub domains are considered in this case. The case shown in Fig. 4.15(a) is 5 sub domains modeling as shown in Fig. 4.9(a), but Fig. 4.15(b) shows 16 sub domain modeling case. The extract directions of the plate-like topology optimization are all $x-$direction. Information of the topology

optimization parameters is summarized in the following.

- **Optimization information**

Stiffness of the spring element k_0: 1×10^5

Upper bound of volume constraint V^*: $0.25\times V^0$

Lower bound of 1st eigenvalue $(\omega_1^*)^2$: $2\times\pi\times(50\ Hz)$

Upper bound of load sum $S(\boldsymbol{\mu})$: 2.0

Upper bound of explicit penalty function δ: 1.4

Filter radius $r_{\min}$: 75 (1.5 times of the average element size)

The result in Fig. 4.16(a) shows that optimal loading point is determined at m^{14} position, but that in Fig. 4.16(b) represent the loading point determination at m^{16} location. It means that the optimal loading location and structural topology depend on sub domain numbers in the plate-like topology optimization method. A couple of parameter studies may be required for the best selection of the sub domains. It can be also regarded as a design option according to the manufacturing strategy or design concept. The structural topological layouts in Fig. 4.16(a) are somewhat similar to those depicted in Fig. 4.10(b), but the front part of the frame structure is completely different due to the different loading location of the cylinder load. Moreover, structural layouts in Fig. 4.16(b) demonstrate new design of a wheel loader frame using the proposed method. Therefore, from the above examples, it can be successfully shown that simultaneous optimization of a loading location and structural topology can provide new design concept with enhanced

performance and the plate-like optimization method helps interpret the result of the topology optimization to the detailed welded structure more effectively.

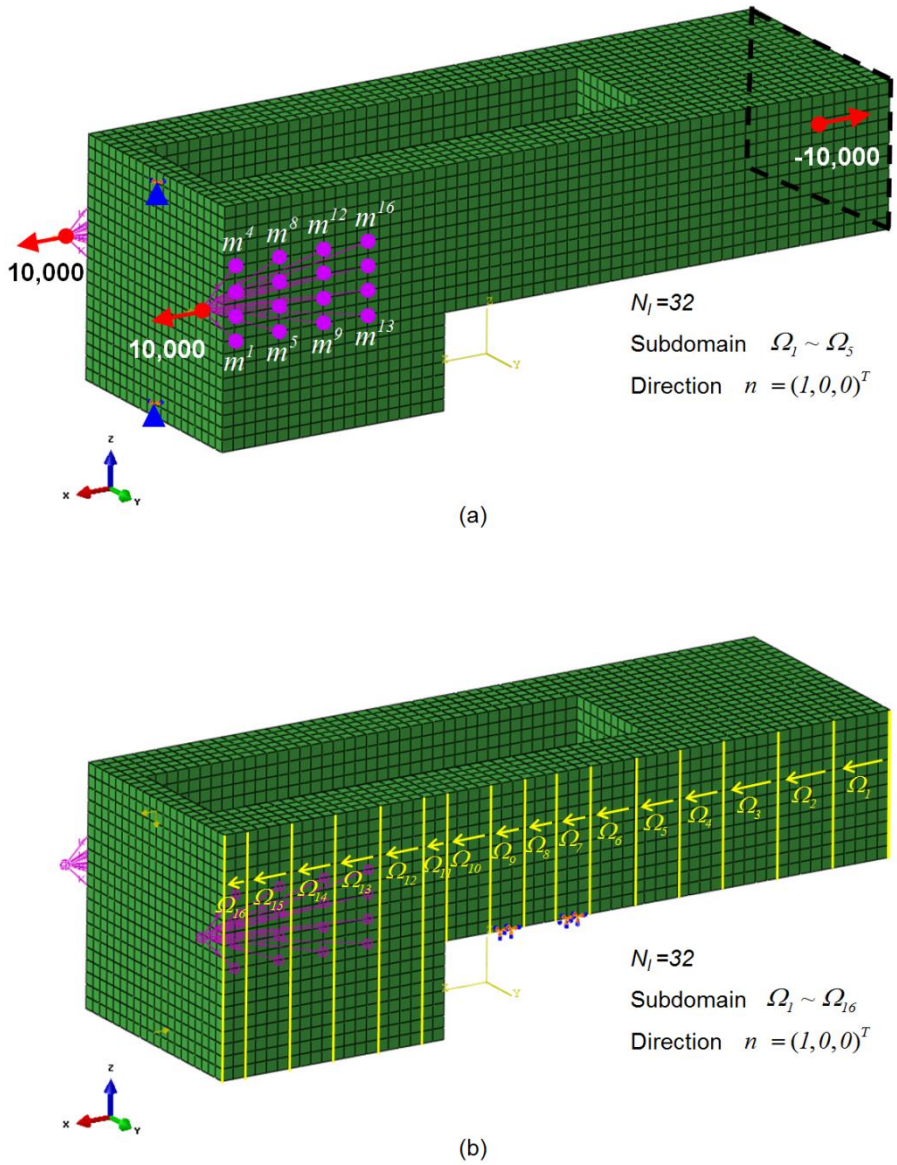

Fig. 4.15 Case study 2 for the integrated topology optimization; a simplified wheel loader frame design in Fig. 4.9.

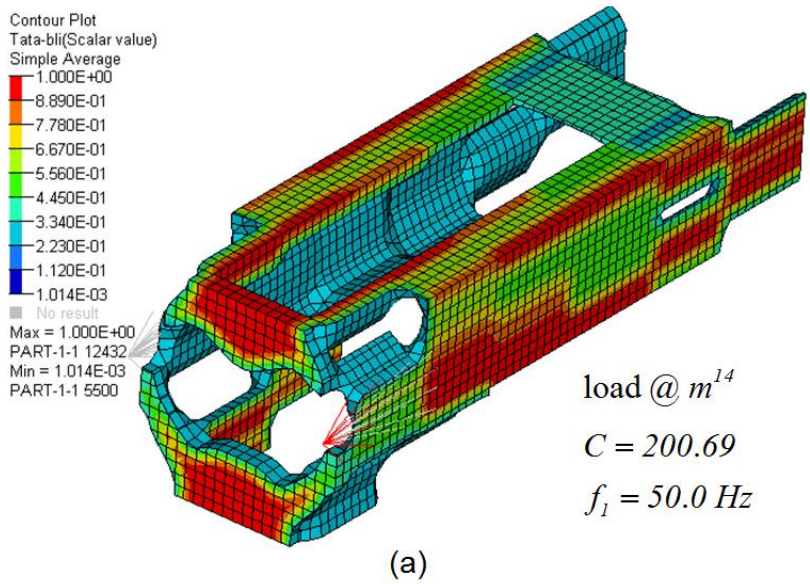

Fig. 4.16 The result of the integrated topology optimization for case study 2: a simplified wheel loader frame case with (a) 7 sub domains, and (b) 16 sub domains.

Chapter 5.

Conclusion

In this work, integrated topology optimization method to cope with two major structural design issues for the construction equipment, such as a wheel loader frame, was investigated. Simultaneous optimization method of a loading location and structural topology for the optimal design of the frame structure hosting an actuator was integrated with the so-called plate-like topology optimization to deal with the manufacturing issue for the welded structure. The effectiveness and usefulness of the proposed method was demonstrated with the design problem of simplified wheel loader frame motivated from an actual engineering practice. The summary of details is presented in the following.

First, a method to find simultaneously the optimal structural topological layout and the loading location for a load of a given magnitude and direction was newly developed. Unlike previous studies focused on movable loads along a designated path line, the proposed method considered an applied load possibly moving around in the designated design domain. The key idea in the proposed approach was to conceptually decouple the loading design domain and the structural design domain. The former was used to determine the loading location by varying the stiffness of the spring elements connecting the applied load and a target node in the design domain and the latter, to determine the optimal structural topological layouts by varying the element density of the structural design domain.

In the proposed approach, the applied load and the candidate loading nodes were assumed to be connected through spring elements the stiffness of which is interpolated by the topological design variable. Because the applied load can move virtually to any nodes in the load design domain, the simple-minded direct connection of the load to the candidate loading node will produce additional unwanted resultants such as a moment. It was shown that if the connecting stiffness has the non-vanishing component only in the direction parallel to the direction of applied load so that only the displacement components in the direction at the candidate nodes are allowed to exist, the applied load can be correctly transferred to the desired node of the structural domain. Also the functional form of the objective function, which is given by the product of the compliance of the connecting springs and that of the structural layouts, was carefully selected; the selected logarithm function adaptively balanced the sensitivities of the two dissimilar compliances. Several case studies in two-dimensional domain were tested with various movable load conditions - the applied vertical load can move vertically, horizontally or arbitrarily within a designated domain. As a specific problem, the design of a simplified wheel loader frame and the determination of the actuator location in the frame, which is a new problem motivated directly from industrial applications, were made simultaneously and the optimized result was found to be consistent with the optimized one obtained by an extensive search with varying possible loading locations. Extension of the developed method to the case studies in the three-dimensional design domain was then verified. Although the developed simultaneous optimization was based on the gradient-based method which cannot guarantee the global optimum solution and had some tuning parameters, possibilities to the practical application were validated by

the above mentioned case studies.

Thereafter, topology optimization considering weld manufacturability was achieved with the extraction of plate-like topological layouts, generated by projecting the design variables in the structural domain to the pre-determined plane of the sub domains in the domain, to the given directions. In the method, mesh-independent nodal design variables were used. The results of the design examples showed practically more effective material layouts to be interpreted to the welded structure than those of the standard topology optimization in spite of a trade-off between manufacturability and structural performance. Moreover, computational cost of the plate-like topology optimization could be somewhat lower because the number of design variables was reduced due to the projection method on the plane of sub domains.

Finally, the simultaneous optimization method of a loading location and structural topology was put together with the plate-like topology optimization method. The developed topology optimization methods were implemented using the interface between *Matlab* and *Abaqus* for the effective application to the practical large-scale problem, such as the structural design of a construction equipment frame. The usefulness of the integrated topology optimization code was validated by a couple of design examples one of which was the problem of a simplified wheel loader frame. The structural layouts of the optimized result showed the possibilities of the new frame design that can be interpreted to the welded structure, which could not be efficiently expected otherwise. From the success in this kind of problem, the proposed integrated topology optimization

method could pave the way for practical engineering applications. This work can also be utilized to the concept design of a welded structure hosting an actuator as well as of a construction equipment frame.

Appendix A.

Numerical studies in the simultaneous optimization of a loading location and structural topology

A.1. Parameter study for the spring stiffness and the explicit penalty constraint

There are two tuning parameters in the simultaneous optimization formulation for a loading location and structural topology. They are nominal spring stiffness k_0 in Eq. (3.1) and the upper bound δ of the explicit penalty constraint function in Eq. (3.12). The results from wide range of parameter studies for the proper selection of these tuning parameters are summarized in Figs. A.1~A.4., indicating successful optimization the blue colored combination. Red colored combinations mean bad results of optimization. The parameter studies are performed for the case studies described in section 3.4. Without loss of generality, the value of k_0 is scaled with the maximum value of the diagonal stiffness k_s in the continuum element. The suggested values of these parameters are in the following:

- The upper bound δ is dependent to the problem definition. But, the value of 0.3 or 0.8 yields satisfactory results generally.
- The value of k_0 ranges between 1 to 10^{-4} times smaller than the diagonal stiffness of the continuum element yields satisfactory results always if δ is properly chosen, but the value lower than $0.1k_s$ is suggested because the spring element can perturb the stiffness in the continuum domain otherwise.

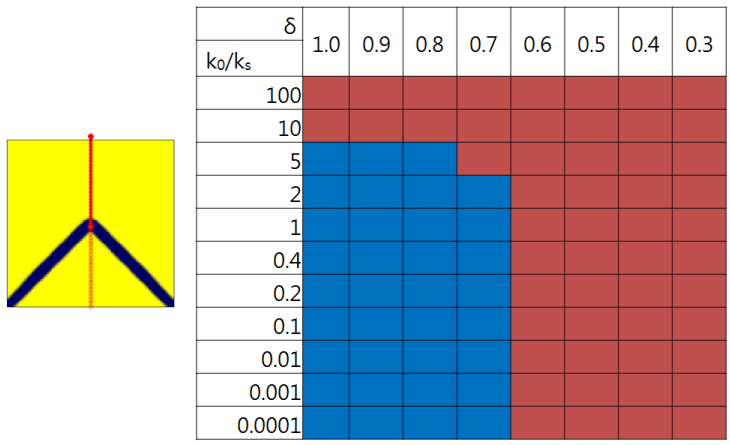

Fig. A.1 Parameter study results of the tuning parameters, k_0 and δ, for the example in Fig. 3.4

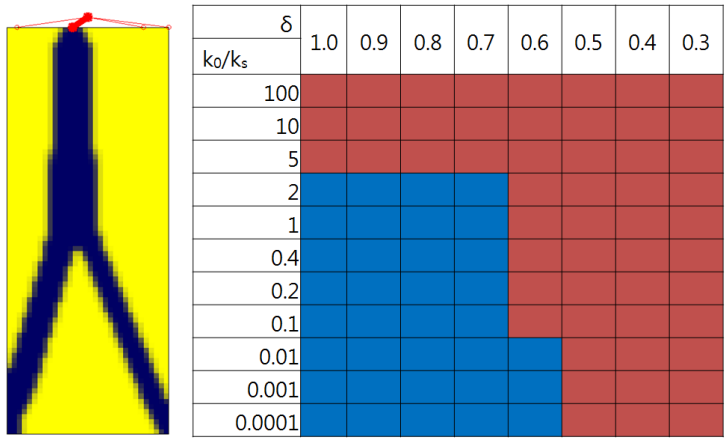

Fig. A.2 Parameter study results of the tuning parameters, k_0 and δ, for the example in Fig. 3.6

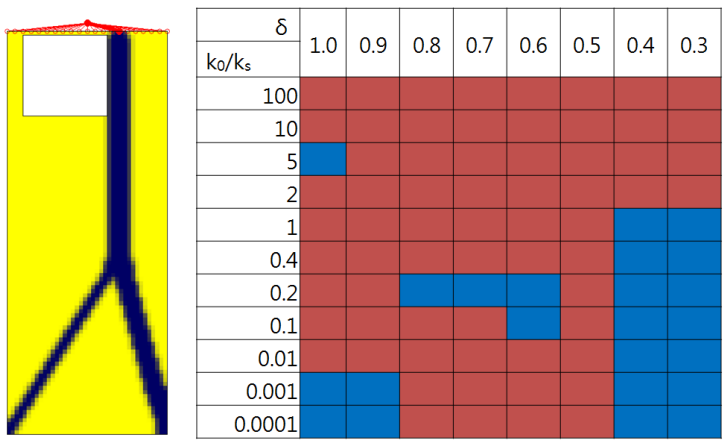

Fig. A.3 Parameter study results of the tuning parameters, k_0 and δ, for the example in Fig. 3.8

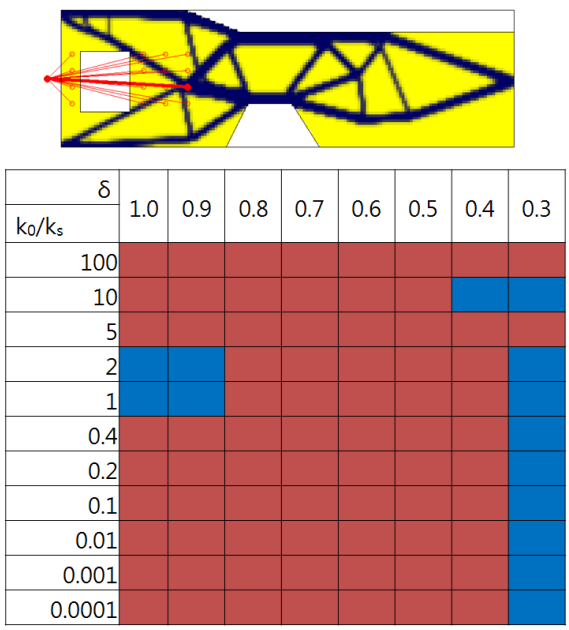

Fig. A.4 Parameter study results of the tuning parameters, k_0 and δ, for the example in Fig. 3.10

A.2. Standard topology optimization results under pre-determined loading for the 2D wheel loader case in Fig. 3.10

All of the results investigated by the standard topology optimization for the pre-determined load applied at every candidate loading locations are summarized in Fig. A.5 ~A.6. The entire results have 16 topology optimization sets and the efficiency of the proposed simultaneous optimization can be calculated directly from the sum of cost of the entire pre-determined loading cases.

- Sum of the cost for all of pre-determined loading: *13,583 sec*
- Simultaneous optimization of a loading point and structural topology: *1,650 sec*

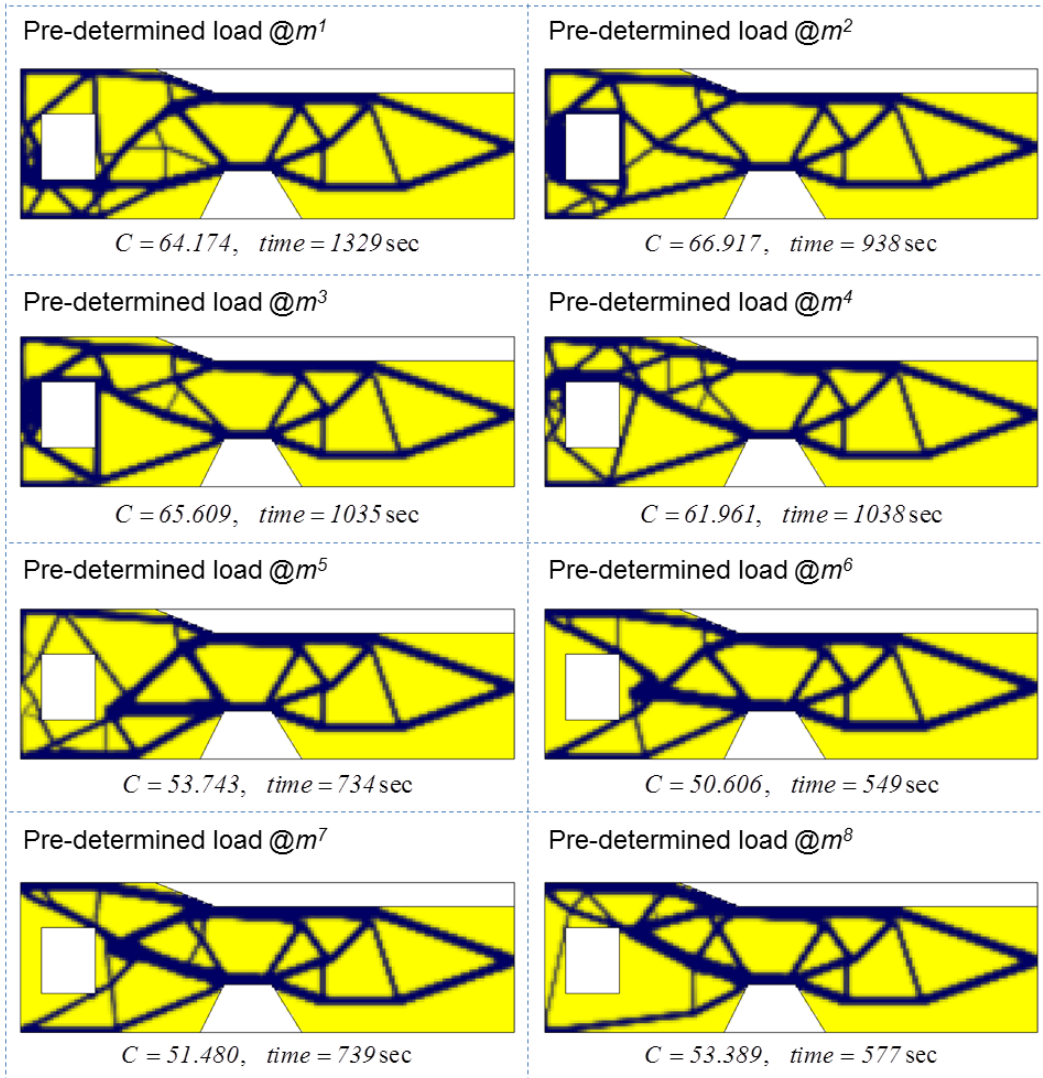

Fig. A.5 Standard topology optimization results under pre-determined loading for the 2D wheel loader case in Fig. 3.10: $m^1 \sim m^8$

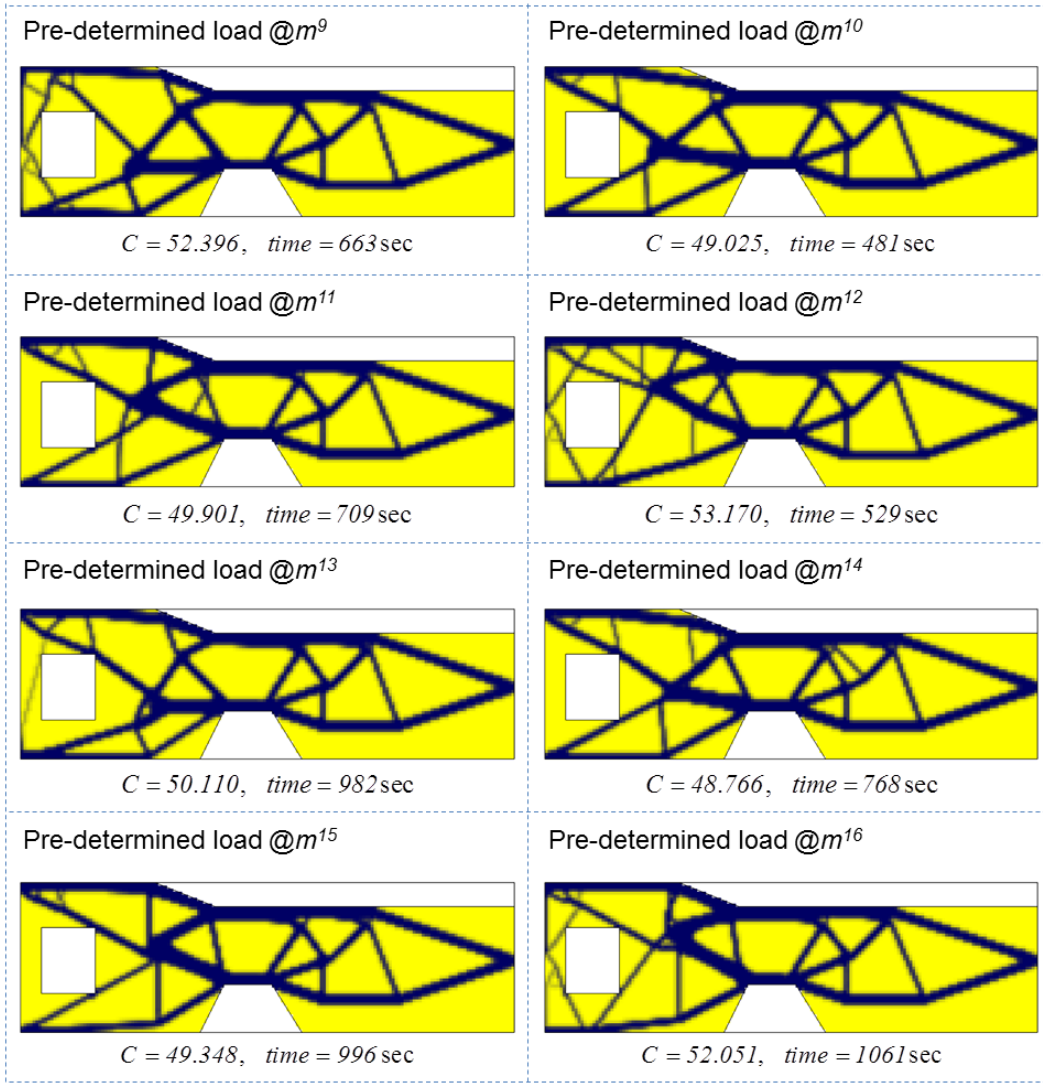

Fig. A.6 Standard topology optimization results under pre-determined loading for the 2D wheel loader case in Fig. 3.10: $m^9 \sim m^1$

Appendix B.

Case studies of the simultaneous optimization of multiple loading locations and structural topology

Case studies for the multiple loading determination problems will be demonstrated in this section. Two kind of typical example are as follows.

B.1. Two optimal loading locations under symmetric condition

The problem depicted in Fig. B.1(a) is the same structural design domain with extended loading domain. The loading domain is composed of 189 possible loading points inside the structural design domain. The applied load is acting vertically. Informations of finite element modeling, material properties and optimization parameters are listed below.

- The bottom side ends are simply supported.
- The structural domain: 96×96 4-node plane stress elements. Thickness=10 mm.
- Young's modulus $E_0 = 210$ GPa and Poisson's ratio ν =0.3.
- Candidate loading points are horizontally equally spaced from the 33^{th} node to the 65^{th} node to the positive x-direction so as to be totally 9 candidate points in the x-direction.
- Candidate loading points are vertically equally spaced from y=0 to y=1000 to the positive y-direction so as to be totally 21 candidate points in the y-direction.
- The nominal value of k_0 is 10^{-1} times smaller than the diagonal stiffness of the

continuum element.

- The constraint are $\overline{V^*} = 10\%$ and $S(\boldsymbol{\mu}) \le 1$
- Density filter with filter radius, rmin=2.
- Initial values of all design variables are set to be $\rho_i = \overline{V^*}$ and $\mu_i = 1/N_l$.
- The upper bound value of $\delta = 0.7$. This value should be selected to be feasible if load design variables converges to the value, $\mu_i = 0.5$ and $\mu_j = 0.5$,$(i \neq j)$.

Figure B.1(b) shows the optimization results. Note that $\mu_6 = 0.5$ and $\mu_{110} = 0.5$. The structural compliance in the structural domain is much lower than the value in Fig. 3.4(b) (2.361 vs. 3.299). This is evident because distributed load is more favorable for the structural compliance.

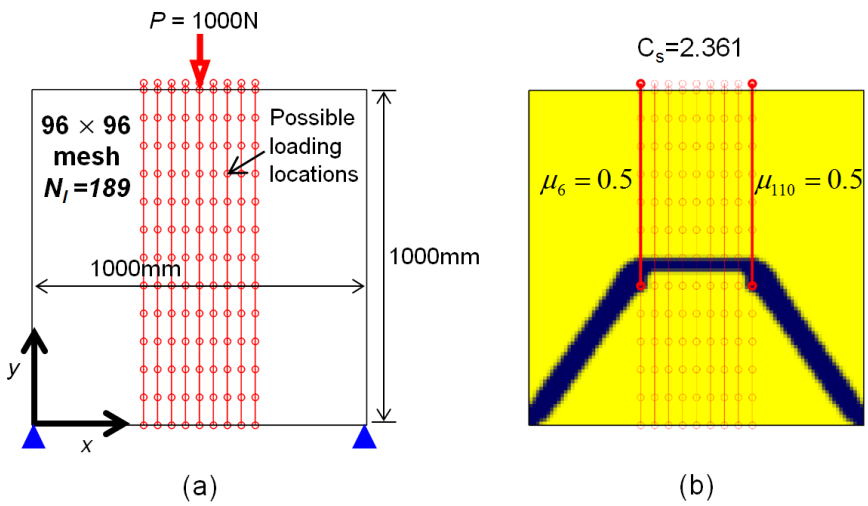

Fig. B.1 Two optimal loading points under symmetric loading condition: (a) Design domain with prescribed load/boundary conditions, (b) the result by the proposed simultaneous optimization method.

B.2. Two optimal loading locations determination problem

The problem depicted in Fig. B.2(a) is the design domains for the two optimal loading locations determination. In the symmetric model or simple loading model, the optimal loading points tend to be split into outside locations; therefore, special design domain is as devised as the optimal loading points to be split. The loading domain is composed of 26 possible loading points on the top line of the structural design domain. The applied load is acting vertically. Informations of finite element modeling, material properties and optimization parameters are listed below. Data are the same as the case study B.1, unless otherwise specified.

- The structural domain: 100×50 4-node plane stress elements.
- Candidate loading points are horizontally equally spaced from x=0 to x=2000 on the top line (y=1000) to the positive x-direction so as to be totally 26 candidate points in the x-direction.
- Non-design domain: X_1=(0, 500), X_2=(700, 900), X_3=(1200, 500), X_4=(1600, 900)
- Candidate loading points are vertically equally spaced from y=0 to y=1000 to the positive y-direction so as to be totally 21 candidate points in the y-direction.
- The constraint are $\overline{V^*} = 30\%$ and $S(\boldsymbol{\mu}) \le 2$
- Density filter with filter radius, rmin=1.3.
- The upper bound value of $\delta = 0.6$. This value should be relaxed because two loading points are to be determined.

Figure B.2(b) shows the optimization results. Note that μ_{15}=1.0 and μ_{24}=1.0. Note that while the load design variables are equally converged to 1.0, the loads transmitted by the load design variable are different due to the support condition. The load transmitted by the μ_{15} is about 374 and μ_{24}, 626.

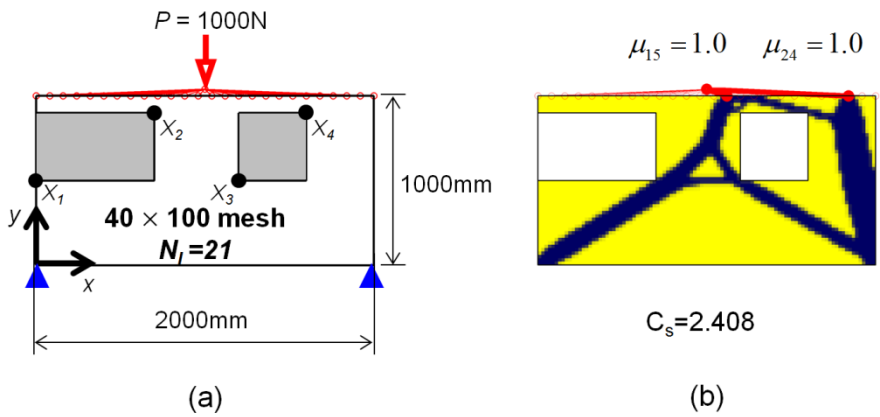

Fig. B.2 Two optimal loading points under two applied load: (a) Design domain with prescribed load/boundary conditions, (b) the result by the proposed simultaneous optimization method.

References

[1] Bendsøe, M.P., *Optimal shape design as a material distribution problem.* Structural Optimization, 1989. **1**(4): p. 193-202.

[2] Bendsøe, M.P. and N. Kikuchi, *Generating optimal topologies in structural design using a homogenization method*. Computer Methods in Applied Mechanics and Engineering, 1988. **71**(2): p. 197-224.

[3] Zhou, M. and G.I.N. Rozvany, *The COC algorithm, Part II: topological, geometrical and generalized shape optimization.* Computer Methods in Applied Mechanics and Engineering, 1991. **89**(1): p. 309-336.

[4] Bendsøe, M.P. and O. Sigmund, *Topology optimization: theory, methods and applications*. 2003: Springer, Berlin.

[5] Cavazzuti, M., et al., *High performance automotive chassis design: a topology optimization based approach.* Structural and Multidisciplinary Optimization, 2011. **44**(1): p. 45-56.

[6] Deaton, J.D. and R.V. Grandhi, *A survey of structural and multidisciplinary continuum topology optimization: post 2000*. Structural and Multidisciplinary Optimization, 2013. **49**(1): p. 1-38.

[7] Du, J. and N. Olhoff, *Topological design of freely vibrating continuum structures for maximum values of simple and multiple eigenfrequencies and frequency gaps*. Structural and Multidisciplinary Optimization, 2007. **34**(2): p. 91-110.

[8] Forcier, L.C. and S. Joncas, *Development of a structural optimization strategy for the design of next generation large thermoplastic wind turbine blades*. Structural and Multidisciplinary Optimization, 2012. **45**(6): p. 889-906.

[9] Jang, G.W., M.S. Yoon, and J.H. Park, *Lightweight flatbed trailer design by using topology and thickness optimization*. Structural and Multidisciplinary Optimization, 2010. **41**(2): p. 295-307.

[10] Kim, S.I. and Y.Y. Kim, *Topology optimization of planar linkage mechanisms*. International Journal for Numerical Methods in Engineering, 2014. **98**(4): p. 265-286.

[11] Kim, W., Y.H. Song, and J.E. Kim, *Topology optimization of actuator arms in hard disk drives for reducing bending resonance-induced off-tracks*. Structural and Multidisciplinary Optimization, 2012. **46**(6): p. 907-912.

[12] Krog, L., et al. *Topology optimization of aircraft wing box ribs*. in 10th AIAA/ISSMO MAO conference. 2004. Albany.

[13] Pedersen, N.L., *Maximization of eigenvalues using topology optimization*. Structural

and Multidisciplinary Optimization, 2000. **20**(1): p. 2-11.

[14] Remouchamps, A., et al., *Application of a bi-level scheme including topology optimization to the design of an aircraft pylon*. Structural and Multidisciplinary Optimization, 2011. **44**(6): p. 739-750.

[15] Rietz, A., *Weld optimization with stress constraints and thermal load*. Structural and Multidisciplinary Optimization, 2012. **46**(5): p. 755-760.

[16] Rozvany, G.I.N., *Aims, scope, methods, history and unified terminology of computer-aided topology optimization in structural mechanics*. Structural and Multidisciplinary Optimization, 2001. **21**(2): p. 90-108.

[17] Sigmund, O., *On the design of compliant mechanisms using topology optimization*. Journal of Structural Mechanics, 1997. **25**(4): p. 493-524.

[18] Sigmund, O. and K. Maute, *Topology optimization approaches*. Structural and Multidisciplinary Optimization, 2013. **48**(6): p. 1031-1055.

[19] Stromberg, L.L., et al., *Application of layout and topology optimization using pattern gradation for the conceptual design of buildings*. Structural and Multidisciplinary Optimization, 2010. **43**(2): p. 165-180.

[20] Xiao, D., et al., *Application of topology optimization to design an electric bicycle main frame*. Structural and Multidisciplinary Optimization, 2012. **46**(6): p. 913-929.

[21] Yoon, G.H. and Y.Y. Kim, *Element connectivity parameterization for topology optimization of geometrically nonlinear structures*. International Journal of Solids and Structures, 2005. **42**(7): p. 1983-2009.

[22] Zhu, J.H., et al., *Structural topology optimization with constraints on multi-fastener joint loads*. Structural and Multidisciplinary Optimization, 2014. **50**(4): p. 561-571.

[23] Zhu, J.H., W.H. Zhang, and L. Xia, *Topology Optimization in Aircraft and Aerospace Structures Design*. Archives of Computational Methods in Engineering, 2015.

[24] Buhl, T., *Simultaneous topology optimization of structure and supports*. Structural and Multidisciplinary Optimization, 2002. **23**(5): p. 336-346.

[25] Jang, G.W., H.S. Shim, and Y.Y. Kim, *Optimization of support locations of beam and plate structures under self-weight by using a sprung structure model*. Journal of Mechanical Design, 2009. **131**(2): p. 021005.

[26] Fuchs, M.B. and E. Moses, *Optimal structural topologies with transmissible loads*. Structural and Multidisciplinary Optimization, 2000. **19**(4): p. 263-273.

[27] Chiandussi, G., M. Codegone, and S. Ferrero, *Topology optimization with optimality criteria and transmissible loads*. Computers & Mathematics with Applications, 2009. **57**(5): p. 772-788.

[28] Yang, X.Y., Y.M. Xie, and G.P. Steven, *Evolutionary methods for topology optimisation of continuous structures with design dependent loads*. Computers & Structures, 2005. **83**(12-13): p. 956-963.

[29] Rozvany, G.I.N. and W. Prager, *A new class of structural optimization problems: optimal archgrids*. Computer Methods in Applied Mechanics and Engineering, 1979. **19**(1): p. 127-150.

[30] Rozvany, G.I.N. and C.M. Wang, *On plane Prager-structures—I*. International Journal of Mechanical Sciences, 1983. **25**(7): p. 519-527.

[31] Zhang, W.H., et al., *Structural topology optimization: Extensibility and attainability*. Science China Technological Sciences, 2014. **57**(7): p. 1310-1321.

[32] Harzheim, L. and G. Graf, *Topshape: an attempt to create design proposals including manufacturing constraints*. International Journal of Vehicle Design, 2002. **28**(4): p. 389-409.

[33] Leiva, J.P. *A Topology Optimization Method to Extract Optimal Beam-Like, Plate-*

Like, or Shell-Like Structures from a Solid Finite Element Mesh. in 3rd International Conference on Engineering Optimization. 2012. Rio de Janeiro, Brazil.

[34] Leiva, J.P., B.C. Watson, and I. Kosaka. *An analytical bi-directional growth parameterization to obtain optimal castable topology designs*. in 10th AIAA/ISSMO symposium on multidisciplinary analysis and optimization. 2004. Albany, NY.

[35] Zhou, M., et al. *Progress in topology optimization with manufacturing constraints*. in Proceedings of the 9th AIAA MDO conference AIAA-2002-4901. 2002. Atalanta, Georgia.

[36] Altair OptiStruct, *Optistruct 11 User's manual*. Altair Engineering Inc., Troy, MI, www.altair.com

[37] Komatsu, *Wheel Loader Catalog WA320-5*. 2008, Japan.

[38] Volvo Construction Equipment, *Wheel Loader Catalog L250G*. 2010, Seoul, Korea.

[39] Kim, T.S. and Y.Y. Kim, *Multiobjective topology optimization of a beam under torsion and distortion*. AIAA journal, 2002. **40**(2): p. 376-381.

[40] Choi, K.K. and N.H. Kim, *Structural sensitivity analysis and optimization: linear systems*. Vol. 1. 2004: Springer, New York.

[41] Svanberg, K., *The method of moving asymptotes—a new method for structural optimization*. International Journal for Numerical Methods in Engineering, 1987. **24**(2): p. 359-373.

[42] Bruns, T. and D.A. Tortorelli, *Topology optimization of non-linear elastic structures and compliant mechanisms*. Computer Methods in Applied Mechanics and Engineering, 2001. **190**(26): p. 3443-3459.

[43] Guest, J.K., J.H. Prévost, and T. Belytschko, *Achieving minimum length scale in topology optimization using nodal design variables and projection functions*. International Journal for Numerical Methods in Engineering, 2004. **61**(2): p. 238-254.

[44] Sigmund, O. and J. Petersson, *Numerical instabilities in topology optimization: a survey on procedures dealing with checkerboards, mesh-dependencies and local minima*. Structural Optimization, 1998. **16**(1): p. 68-75.

[45] Dassault Systèmes Simulia. *ABAQUS 6.12 Documentation*, Providence, Rhode Island, USA, 2012.

[46] Tcherniak, D., *Topology optimization of resonating structures using SIMP method*. International Journal for Numerical Methods in Engineering, 2002. **54**(11): p. 1605-1622.

Abstract (Korean)

건설기계 프레임의 통합 위상 최적화

곽 성 규

서울대학교 대학원

기계항공공학부

본 논문은 건설기계 프레임 설계 시에 적용할 수 있는 통합 위상 최적화 방법론 개발을 목적으로 한다. 건설기계 프레임의 위상 최적화와 관련하여 두 가지 주요 설계 이슈가 있으며, 이 중 한 가지는 액츄에이터(actuator)의 레이아웃(layout)과 프레임의 구조 위상을 동시에 최적화하는 것이고, 나머지 한 가지는 위상 최적화 결과의 제작 가능성을 확보하기 위한 방법에 대한 것이다. 휠로더(wheel loader)에서의 조향 실린더와 같이, 건설기계에 내장된 액츄에이터는 프레임에 외력을 전달하게 된다. 이 때, 액츄에이터의 위치가 프레임 구조물에서 하중 점으로 작용하기 때문에, 그 위치에 따라 프레임의 구조 최적화 결과가 크게 영향을 받을 수 있다. 또한, 액츄에이터의 배치가 아직 결정되지 않은 프레임의 초기 개념설계 단계에서는, 액츄에이터의 위치가 지정된 설계영역 내부에서 자유롭게 이동할 수 있다. 따라서, 하중의 위치와 구조 위상에 대한 동시 최적화가 필요하며, 본 연구에서는 이를 위한 방법론을 제

안한다. 하중의 위치와 구조 위상의 동시 최적화에 대한 소수의 관련 연구가 있지만, 하중 점이 주어진 선 또는 경계를 따라 이동할 수 있는 경우로만 제한되어 있는 실정이다. 한편, 위상 최적화를 통해 최적화된 레이아웃을 결정한다 하더라도 일반적으로 위상 최적화에 의한 결과는 그 형태가 용접으로 제작하기에 적절하지 않기 때문에, 최적화된 구조를 실제로 용접에 의해 제작할 수 있는지가 주요한 기술 적용의 장애물이 된다. 이런 문제를 해결하기 위하여 판재 형태의 위상 최적화(plate-like topology optimization) 기법, 즉, 특정 평면으로 투영(projection)한 절점 설계변수(nodal design variable)의 위상을 사전에 정해진 방향으로 추출(extraction)하는 방법을 제안한다. 이러한 접근 방법으로 용접 구조물과 유사한 형태의 위상 최적화 결과를 기대할 수 있다.

하중 점의 위치와 구조 위상의 동시 최적화 및 용접 제작 가능성을 고려한 위상 최적화 기법을 개발하고, *Matlab*과 *Abaqus*를 이용하여 통합한다. 다양한 예제를 통하여 제안한 방법론을 검증한 후, 휠로더 프레임의 최적 설계 문제를 통하여 실제 산업계의 공학 문제로의 적용 가능성을 확인한다.

주제어 : 위상 최적화, 동시 최적화, 이동 하중, 강성 설계, 용접 제작성 제한조건

학 번 : 2011-31289